

Efficient causal inference with hidden confounders from genome-transcriptome variation data

Lingfei Wang and Tom Michoel*

Division of Genetics and Genomics, The Roslin Institute
University of Edinburgh, Easter Bush, EH25 9RG, UK

July 17, 2022

Abstract

Natural genetic variation between individuals in a population leads to variations in gene expression that are informative for the inference of gene regulatory networks. Particularly, genome-wide genotype and transcriptome data from the same samples allow for causal inference between gene expression traits using the DNA variations in cis-regulatory regions as causal anchors. However, existing causal inference programs are not efficient enough for contemporary datasets, and unrealistically assume the absence of hidden confounders affecting the coexpression of causally related gene pairs. Here we propose alternative statistical tests to infer causal effects in the presence of confounding and weak regulations, and implemented both the novel and the traditional causal inference tests in the software package Findr (Fast Inference of Networks from Directed Regulations), achieving thousands to millions of times of speedup due to analytical false positive rate estimation and implementational optimizations. A systematic evaluation using simulated data from the DREAM5 Systems Genetics challenge demonstrated that the novel tests outperformed existing causal inference methods as well as all challenge submissions. We confirmed these results using siRNA silencing, ChIP-sequencing and microRNA target data to validate causal gene-gene and microRNA-gene interactions inferred from genotype, microRNA and mRNA sequencing data of nearly 400 human individuals from the Geuvadis study. Findr provides the community with the first efficient and accurate causal inference tool for modern datasets of tens of thousands of RNA expression traits and genotypes from hundreds or more human individuals. Findr is publicly available at <https://github.com/lingfeiwang/findr>.

Contents

1	Introduction	2
2	Methods	3
2.1	Datasets	3
2.2	General inference algorithm	4
2.3	Likelihood ratio tests	4
2.4	Null distributions for the log-likelihood ratios	7
2.5	Bayesian inference of posterior probabilities	10
2.6	Tests to evaluate	11
2.7	Evaluation methods	11

*Corresponding author: Tom.Michoel@roslin.ed.ac.uk

3	Results	12
3.1	Traditional causal inference fails in the presence of hidden confounders and weak regulations	12
3.2	Findr accounts for weak secondary linkage and hidden confounders and outperforms existing methods on simulated data	13
3.3	Findr outperforms multivariate machine learning methods on microRNA target prediction in human lymphoblastoid cells	14
3.4	Findr accurately predicts transcription factor targets in human lymphoblastoid cells .	15
4	Discussion	15
S1	Methods	22
S1.1	Practical details for Bayesian inference	22
S2	Results	22
S2.1	Iterative conditioning conflicts with FPR-based probability estimation	22
S2.2	Analytical null distribution matches random permutations	23
S2.3	Subsampling performances of existing and new causal inference methods on DREAM datasets	23
S2.4	Findr achieves best performance on miRNA target predictions from Geuvadis dataset	23

1 Introduction

Regulation of gene expression by DNA- and RNA-binding proteins and RNAs is one of the fundamental mechanisms by which cells respond to their environment and obtain their cell type specific identity. To understand the complex networks of interactions between genes and their RNA and protein products that control gene regulation at a systems level, statistical network inference methods are essential. These methods typically search for similarity patterns between genes in large-scale, genome-wide datasets measuring gene expression levels in response to cellular perturbations [1–3]. While specific network interventions in the form of gene silencing or activation experiments are desirable for determining causal effects between genes, less specific perturbations such as responses to external cues (e.g. drugs), dynamic processes (e.g. cell cycle, disease progression) or natural genetic variation are more readily available, especially for mammalian systems. Of these, natural genetic variation data is particularly informative. When genome-wide genetic differences as well as gene expression profiles are available for the same individuals, they can facilitate the inference of the causal direction of regulation between correlated genes, based on the principle that genetic variation causes variation in (typically nearby) gene expression [4] and acts as a causal anchor for identifying downstream genes [5, 6]. Although numerous statistical models and tests have been proposed for causal inference with genotype and gene expression data from matching samples [7–13], no software implementation in the public domain is able to handle the volume of datasets which have surged in recent years due to the advent of high-throughput sequencing technologies, particularly in human [14–17]. Moreover, all current statistical models rely on a conditional independence test which assumes that no hidden confounding factors affect the coexpression of causally related gene pairs. However it is well known that gene regulatory networks exhibit a large degree of redundancy [18] and are organized into higher order network motifs [19], suggesting that confounding of causal relations by common upstream regulators is the rule rather than the exception.

To investigate and address these issues, we developed Findr (Fast Inference of Networks from Directed Regulations), a software package that implements existing and novel statistical causal inference tests tailored to take into account the presence of unknown confounding effects. Findr uses analytical formulae for the null distributions of the likelihood ratios of the implemented tests, which replaces computationally expensive random permutations. This, together with implementational optimizations, resulted in thousands to millions of times of speed up compared to existing methods, and allowed a systematic validation of various causal inference tests using the DREAM5 Systems Genetics

Challenge dataset, consisting of simulated genotype and expression profiles of synthetic gene networks of 1000 genes [20]. We found that the novel tests consistently outperformed all submissions to the DREAM challenge, as well as existing causal inference methods based on conditional independence tests, which exhibited a counter-intuitive worse performance as the number of samples increased.

Next we inferred causal gene-gene and microRNA-gene interactions from genotype, mRNA and microRNA (miRNA) sequencing data of lymphoblastoid cell lines of 360 human individuals from the Geuvadis study [14], and validated predictions using siRNA silencing [21] and DNA-binding inferred from DNase footprinting [22] and ChIP-sequencing [23] data of transcription factors in lymphoblastoid cells, and an integrated database of experimentally confirmed miRNA target genes [24]. This confirmed that our novel causal inference method that takes into account confounding effects consistently outperformed classical causal inference methods as well as methods that only rely on gene expression information.

In summary, we have introduced novel statistical tests and computed analytical null distributions to address the pitfalls of existing causal inference methods. The development of Findr provides the community for the first time with a highly efficient and accurate open source software tool for causal inference from large-scale genotype-tissue expression datasets.

2 Methods

2.1 Datasets

We used the following datasets/databases for evaluating causal inference methods:

1. Simulated genotype and transcriptome data of synthetic gene regulatory networks from the DREAM5 Systems Genetics challenge A (DREAM for short) [20], generated by the SysGenSIM software [25]. DREAM provides 15 sub-datasets, obtained by simulating 100, 300, and 999 samples of 5 different networks each, containing 1000 genes in every sub-dataset but more regulations for sub-datasets with higher numbering. In every sub-dataset, each gene has exactly one matching genotype variable. 25% of the genotype variables are cis-expression Quantitative Trait Loci (eQTL), defined in DREAM as: their variation changes the expression level of the corresponding gene directly. The other 75% are trans-eQTLs, defined as: their variation affects the expression levels of only the *downstream targets* of the corresponding gene, but not the gene itself. Because the identities of cis-eQTLs are unknown, we calculated the P-values of genotype-gene expression associations with kruX [26], and kept all genes with a P-value less than 1/750 to filter out genes without cis-eQTL. For the subsampling analysis (detailed in Section 2.7), we restricted the evaluation to the prediction of target genes from these cis-genes only, in line with the assumption that Findr and other causal inference methods require as input a list of genes whose expression is significantly associated with at least one cis-eQTL. For a full comparison of Findr to the DREAM leaderboard results, we predicted target genes for all genes, regardless of whether they had a cis-eQTL.
2. Genotype and transcriptome sequencing data on 465 human lymphoblastoid cell line samples from the Geuvadis project [14] consisting of the following data products:
 - Genotype data [27].
 - Gene quantification data for 23722 genes from nonredundant unique samples and after quality control and normalization [28].
 - Quantification data of miRNA, with the same standard as gene quantification data [29].
 - Best eQTLs of mRNAs and miRNAs [30].

We restricted our analysis to 360 European samples which are shared by gene and miRNA quantifications. Excluding invalid eQTLs from the Geuvadis analysis, such as single-valued genotypes, 55 miRNA-eQTL pairs and 3172 gene-eQTL pairs were retained.

3. For validation of predicted miRNA-gene interactions, we extracted the “strong” ground-truth table from miRLAB [24, 31], which contains experimentally confirmed miRNA-gene regulations

from the following databases: TarBase [32], miRecords [33], miRWalk [34], and miRTarBase [35]. The intersection of the Geuvadis and ground-truth table contains 20 miRNAs and 1054 genes with 1217 confirmed regulations, which are considered for prediction validation. Interactions that are present in the ground-truth table are regarded as true while others as false.

4. For verification of predicted gene-gene interactions, we obtained differential expression data following siRNA silencing of 59 transcription-associated factors (TFs) and DNA-binding data of 201 TFs for 8872 genes in a reference lymphoblastoid cell line (GM12878) from [21]. Six siRNA-targeted TFs, 20 DNA-binding TFs, and 6,790 target genes without missing differential expression data intersected with the set of 3172 eQTL-genes and 23722 target genes in Geuvadis and were considered for validation. We reproduced the pipeline of [21] with the criteria for true targets as having a False Discovery Rate (FDR) < 0.05 from R package *qvalue* for differential expression in siRNA silencing, or having at least 2 TF-binding peaks within 10kb of their transcription start site. We also obtained the filtered proximal TF-target network from [23], which had 14 TFs and 7,000 target genes in common with the Geuvadis data, respectively.

2.2 General inference algorithm

Consider a set of observations sampled from a mixture distribution of a null and an alternative hypothesis. For instance in gene regulation, every observation can correspond to expression levels of a pair of genes which are sampled from a bivariate normal distribution with zero (null hypothesis) or non-zero (alternative hypothesis) correlation coefficient. In Findr, we predict the probability that any sample follows the alternative hypothesis with the following algorithm (based on and modified from [8]):

1. For robustness against outliers, we convert every continuous variable into standard normally distributed $N(0, 1)$ values using a rank-based inverse normal transformation across all samples. We name this step as *supernormalization*.
2. We propose a null and an alternative hypothesis for every likelihood ratio test (LRT) of interest where, by definition, the null hypothesis space is a subset of the alternative hypothesis. Model parameters are replaced with their maximum likelihood estimators (MLEs) to obtain the log likelihood ratio (LLR) between the alternative and null hypotheses (Section 2.3).
3. We derive the analytical expression for the probability density function (PDF) of the LLR when samples follow the null hypothesis (Section 2.4).
4. We convert LLRs into posterior probabilities of the hypothesis of interest with empirical false positive rate (FPR) estimation. This is achieved by first estimating the proportion of null hypothesis and then performing Bayesian inference (Section 2.5).

Implementational details can be found in Findr’s source code.

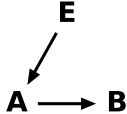
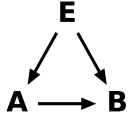

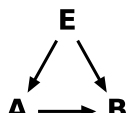


2.3 Likelihood ratio tests

Consider correlated genes A , B , and a third variable E upstream of A and B , such as a significant eQTL of A . The eQTLs can be obtained either *de novo* using eQTL identification tools such as matrix-eQTL [36] or kruX [26], or from published analyses. Throughout this article, we assume that E is a significant eQTL of A , whereas extension to other data types is straightforward. We use A_i and B_i for the expression levels of gene A and B respectively, which are assumed to have gone through the supernormalization in Section 2.2, and optionally the genotypes of the best eQTL of A as E_i , where $i = 1, \dots, n$ across samples. Genotypes are assumed to have a total of n_a alleles, so $E_i = 0, \dots, n_a$. We define the null and alternative hypotheses for a total of six tests, as shown in Table 1. LLRs of every test are calculated separately as follows:

0. **Correlation test:** Define the null hypothesis as A and B are independent, and the alternative hypothesis as they are correlated:

$$\mathcal{H}_{\text{null}}^{(0)} = A \quad B, \quad \mathcal{H}_{\text{alt}}^{(0)} = A \text{ --- } B. \quad (1)$$

Table 1: Six LRTs are performed to test the regulation $A \rightarrow B$. They are numbered, named, and defined in the table below. E is the best eQTL of A . Arrows in a hypothesis indicate directed regulatory relations. Genes A and B each follows a normal distribution, whose mean depends additively on its regulator(s), as determined in the corresponding hypothesis. The dependency is categorical on discrete regulators (genotype) and linear on continuous regulators (gene expression level). Undirected lines represent a multi-variate normal distribution between the relevant variables. In order to identify $A \rightarrow B$ regulation, we select either the null or the alternative hypothesis depending on the test, as shown in the table.

Test ID	Test name	Null (hypothesis)	Alternative (hypothesis)	Selected hypothesis
0	Correlation	A B	A — B	Alternative
1	Primary (linkage)	E A	E → A	Alternative
2	Secondary (linkage)	E B	E → B	Alternative
3	(Conditional) Independence			Null
4	Relevance			Alternative
5	Controlled			Alternative

The superscript (0) is the numbering of the test. Both hypotheses are modeled with gene expression levels following bivariate normal distributions, as

$$\begin{pmatrix} A_i \\ B_i \end{pmatrix} \sim N \left(\begin{pmatrix} 0 \\ 0 \end{pmatrix}, \begin{pmatrix} \sigma_{A0}^2 & \rho \sigma_{A0} \sigma_{B0} \\ \rho \sigma_{A0} \sigma_{B0} & \sigma_{B0}^2 \end{pmatrix} \right),$$

for $i = 1, \dots, n$. The null hypothesis corresponds to $\rho = 0$.

Maximum likelihood estimators (MLE) for the model parameters ρ , σ_{A0} , and σ_{B0} are

$$\hat{\rho} = \frac{1}{n} \sum_{i=1}^n A_i B_i, \quad \hat{\sigma}_{A0} = \hat{\sigma}_{B0} = 1, \quad (2)$$

and the LLR is simply

$$\text{LLR}^{(0)} = -\frac{n}{2} \ln(1 - \hat{\rho}^2). \quad (3)$$

In the absence of genotype information, we use nonzero correlation between A and B as the indicator for $A \rightarrow B$ regulation, giving the posterior probability

$$P(A \rightarrow B) = P(\mathcal{H}_{\text{alt}}^{(0)} \mid \text{LLR}^{(0)}).$$

false negative

1. **Primary (linkage) test:** Verify that E regulates A from $\mathcal{H}_{\text{alt}}^{(1)} \equiv E \rightarrow A$ and $\mathcal{H}_{\text{null}}^{(1)} \equiv E \not\rightarrow A$. For $\mathcal{H}_{\text{alt}}^{(1)}$, we model $E \rightarrow A$ as A follows a normal distribution whose mean is determined by E categorically, i.e.

$$A_i \mid E_i \sim N(\mu_{E_i}, \sigma_A^2). \quad (4)$$

From the total likelihood $p(A \mid E) = \prod_{i=1}^n p(A_i \mid E_i)$, we find MLEs for model parameters $\mu_j, j = 0, 1, \dots, n_a$, and σ_A , as

$$\hat{\mu}_j = \frac{1}{n_j} \sum_{i=1}^n A_i \delta_{E_{ij}}, \quad \hat{\sigma}_A^2 = 1 - \sum_{j=0}^{n_a} \frac{n_j}{n} \hat{\mu}_j^2,$$

where n_j is the sample count by genotype category,

$$n_j \equiv \sum_{i=1}^n \delta_{E_{ij}}.$$

The Kronecker delta function is defined as $\delta_{xy} = 1$ for $x = y$, and 0 otherwise. When summing over all genotype values ($j = 0, \dots, n_a$), we only pick those that exist ($n_j > 0$) throughout this article. Since the null hypothesis is simply that A_i is sampled from a genotype-independent normal distribution, with MLEs of mean zero and standard deviation one due to the supernormalization (Section 2.2), the LLR for test 1 becomes

$$\text{LLR}^{(1)} = -\frac{n}{2} \ln \hat{\sigma}_A^2. \quad (5)$$

By favoring a large $\text{LLR}^{(1)}$, we select $\mathcal{H}_{\text{alt}}^{(1)}$ and verify that E regulates A , with

$$P(E \rightarrow A) = P(\mathcal{H}_{\text{alt}}^{(1)} \mid \text{LLR}^{(1)}).$$

2. **Secondary (linkage) test:** The secondary test is identical with the primary test, except it verifies that E regulates B . Hence repeat the primary test on E and B and obtain the MLEs:

$$\hat{\nu}_j = \frac{1}{n_j} \sum_{i=1}^n B_i \delta_{E_{ij}}, \quad \hat{\sigma}_B^2 = 1 - \sum_{j=0}^{n_a} \frac{n_j}{n} \hat{\nu}_j^2,$$

and the LLR as

$$\text{LLR}^{(2)} = -\frac{n}{2} \ln \hat{\sigma}_B^2.$$

$\mathcal{H}_{\text{alt}}^{(2)}$ is chosen to verify that E regulates B .

3. **(Conditional) independence test:** Verify that E and B are independent when conditioning on A . This can be achieved by comparing $\mathcal{H}_{\text{alt}}^{(3)} \equiv B \leftarrow E \rightarrow A \wedge (A \text{ correlates with } B)$ against $\mathcal{H}_{\text{null}}^{(3)} \equiv E \rightarrow A \rightarrow B$. LLRs close to zero then prefer $\mathcal{H}_{\text{null}}^{(3)}$, and ensure that E regulates B only through A :

$$P(E \perp B \mid A) = P(\mathcal{H}_{\text{null}}^{(3)} \mid \text{LLR}^{(3)}).$$

For $\mathcal{H}_{\text{alt}}^{(3)}$, the bivariate normal distribution dependent on E can be represented as

$$\begin{pmatrix} A_i \\ B_i \end{pmatrix} \Big| E_i \sim N \left(\begin{pmatrix} \mu_{E_i} \\ \nu_{E_i} \end{pmatrix}, \begin{pmatrix} \sigma_A^2 & \rho\sigma_A\sigma_B \\ \rho\sigma_A\sigma_B & \sigma_B^2 \end{pmatrix} \right).$$

For $\mathcal{H}_{\text{null}}^{(3)}$, the distributions follow Eq 4, as well as

$$B_i \mid A_i \sim N(\rho A_i, \sigma_B^2).$$

Substituting parameters $\mu_j, \nu_j, \sigma_A, \sigma_B, \rho$ of $\mathcal{H}_{\text{alt}}^{(3)}$ and $\mu_j, \rho, \sigma_A, \sigma_B$ of $\mathcal{H}_{\text{null}}^{(3)}$ with their MLEs, we obtain the LLR:

$$\begin{aligned} \text{LLR}^{(3)} &= -\frac{n}{2} \ln(\hat{\sigma}_A^2 \hat{\sigma}_B^2 - (\hat{\rho} + \sigma_{AB} - 1)^2) \\ &\quad + \frac{n}{2} \ln \hat{\sigma}_A^2 + \frac{n}{2} \ln(1 - \hat{\rho}^2), \end{aligned} \quad (6)$$

where

$$\sigma_{AB} \equiv 1 - \sum_{j=0}^{n_a} \frac{n_j}{n} \hat{\mu}_j \hat{\nu}_j,$$

and $\hat{\rho}$ is defined in Eq 2.

4. **Relevance test:** Since the indirect regulation $E \rightarrow B$ tends to be weaker than any of its direct regulation components ($E \rightarrow A$ or $A \rightarrow B$), we propose to test $E \rightarrow A \rightarrow B$ with indirect regulation $E \rightarrow B$ as well as the direct regulation $A \rightarrow B$ for stronger distinguishing power on weak regulations. We define $\mathcal{H}_{\text{alt}}^{(4)} \equiv E \rightarrow A \wedge E \rightarrow B \leftarrow A$ and $\mathcal{H}_{\text{null}}^{(4)} \equiv E \rightarrow A \rightarrow B$. This simply verifies that B is not independent from both A and E simultaneously. In the alternative hypothesis, B is regulated by E and A , which is modeled as a normal distribution whose mean is additively determined by E categorically and A linearly, i.e.

$$B_i \mid E_i, A_i \sim N(\nu_{E_i} + \rho A_i, \sigma_B^2).$$

We can hence solve its LLR as

$$\text{LLR}^{(4)} = -\frac{n}{2} \ln(\hat{\sigma}_A^2 \hat{\sigma}_B^2 - (\hat{\rho} + \sigma_{AB} - 1)^2) + \frac{n}{2} \ln \hat{\sigma}_A^2.$$

5. **Controlled test:** Based on the positives of the secondary test, we can further distinguish the alternative hypothesis $\mathcal{H}_{\text{alt}}^{(5)} \equiv B \leftarrow E \rightarrow A \wedge A \rightarrow B$ from the null $\mathcal{H}_{\text{null}}^{(5)} \equiv B \leftarrow E \rightarrow A$ to verify that E does not regulate A and B independently. Its LLR can be solved as

$$\text{LLR}^{(5)} = -\frac{n}{2} \ln(\hat{\sigma}_A^2 \hat{\sigma}_B^2 - (\hat{\rho} + \sigma_{AB} - 1)^2) + \frac{n}{2} \ln \hat{\sigma}_A^2 \hat{\sigma}_B^2.$$

2.4 Null distributions for the log-likelihood ratios

The null distribution of LLR, $p(\text{LLR} \mid \mathcal{H}_{\text{null}})$, may be obtained either by simulation or analytically. Simulation, such as random permutations from real data or the generation of random data from statistics of real data, can deal with a much broader range of scenarios in which analytical expressions are unattainable. However, the drawbacks are obvious: simulation can take hundreds of times longer than analytical methods to reach a satisfiable precision. Here we obtained analytical expressions of $p(\text{LLR} \mid \mathcal{H}_{\text{null}})$ for all the tests introduced above.

0. **Correlation test:** $\mathcal{H}_{\text{null}}^{(0)} = A \quad B$ indicates no correlation between A and B . Therefore, we can start from

$$\tilde{B}_i \sim \text{i.i.d } N(0, 1). \quad (7)$$

In order to simulate the supernormalization step, we normalize \tilde{B}_i into B_i with zero mean and unit variance as:

$$B_i \equiv \frac{\tilde{B}_i - \bar{\tilde{B}}}{\sigma_{\tilde{B}}}, \quad \bar{\tilde{B}} \equiv \frac{1}{n} \sum_{i=1}^n \tilde{B}_i, \quad \sigma_{\tilde{B}}^2 \equiv \frac{1}{n} \sum_{i=1}^n (\tilde{B}_i - \bar{\tilde{B}})^2. \quad (8)$$

Transform the random variables $\{\tilde{B}_i\}$ by defining

$$X_1 \equiv \frac{1}{\sqrt{n}} \sum_{i=1}^n A_i \tilde{B}_i, \quad (9)$$

$$X_2 \equiv \frac{1}{\sqrt{n}} \sum_{i=1}^n \tilde{B}_i, \quad (10)$$

$$X_3 \equiv \left(\sum_{i=1}^n \tilde{B}_i^2 \right) - X_1^2 - X_2^2. \quad (11)$$

Since $\tilde{B}_i \sim \text{i.i.d } N(0, 1)$ (according to Eq 7), we can easily verify that X_1, X_2, X_3 are independent, and

$$X_1 \sim N(0, 1), \quad X_2 \sim N(0, 1), \quad X_3 \sim \chi^2(n-2). \quad (12)$$

Expressing Eq 3 in terms of X_1, X_2, X_3 gives

$$\text{LLR}^{(0)} = -\frac{n}{2} \ln(1 - Y), \quad (13)$$

in which

$$Y \equiv \frac{X_1^2}{X_1^2 + X_3} \sim \text{Beta}\left(\frac{1}{2}, \frac{n-2}{2}\right) \quad (14)$$

follows the Beta distribution.

We define distribution $\mathcal{D}(k_1, k_2)$ as

$$-\frac{1}{2} \ln(1 - Y) \sim \mathcal{D}(k_1, k_2),$$

for $Y \sim \text{Beta}(k_1, k_2)$. The probability density function (PDF) for $z \sim \mathcal{D}(k_1, k_2)$ can be derived as: for $z > 0$,

$$p(z | k_1/2, k_2/2) = \frac{2}{B(k_1/2, k_2/2)} (1 - e^{-2z})^{(k_1/2-1)} e^{-k_2 z}, \quad (15)$$

and for $z \leq 0$, $p(z | k_1, k_2) = 0$. Here $B(a, b)$ is the Beta function. Therefore the null distribution for the correlation test is simply

$$\text{LLR}^{(0)}/n \sim \mathcal{D}(1, n-2). \quad (16)$$

1. **Primary test:** $\mathcal{H}_{\text{null}}^{(1)} = E \quad A$ indicates no regulation from E to A . Therefore, similarly with the correlation test, we start from $\tilde{A}_i \sim \text{i.i.d } N(0, 1)$ and normalize them to A_i with zero mean and unit variance.

The expression of $\text{LLR}^{(1)}$ then becomes:

$$\text{LLR}^{(1)} = -\frac{n}{2} \ln \left(1 - \sum_{j=0}^{n_a} \frac{n_j}{n} \frac{(\hat{\mu}_j - \bar{\tilde{A}})^2}{\sigma_{\tilde{A}}^2} \right),$$

where

$$\hat{\mu}_j \equiv \frac{1}{n_j} \sum_{i=1}^n \tilde{A}_i \delta_{E_{ij}}.$$

For now, assume all possible genotypes are present, i.e. $n_j > 0$ for $j = 0, \dots, n_a$. Transform $\{\tilde{A}_i\}$ by defining

$$\begin{aligned} X_j &\equiv \sqrt{n_j} \hat{\mu}_j, & \text{for } j = 0, \dots, n_a, \\ X_{n_a+1} &\equiv \left(\sum_{i=1}^n \tilde{A}_i^2 \right) - \left(\sum_{j=0}^{n_a} X_j^2 \right). \end{aligned} \quad (17)$$

Then we can similarly verify that $\{X_i\}$ are pairwise independent, and

$$\begin{aligned} X_i &\sim N(0, 1), \text{ for } i = 0, \dots, n_a, \\ X_{n_a+1} &\sim \chi^2(n - n_a - 1). \end{aligned} \quad (18)$$

Again transform $\{X_i\}$ by defining independent random variables

$$\begin{aligned} Y_1 &\equiv \sum_{j=0}^{n_a} \sqrt{\frac{n_j}{n}} X_j \sim N(0, 1), \\ Y_2 &\equiv \left(\sum_{j=0}^{n_a} X_j^2 \right) - Y_1^2 \sim \chi^2(n_a), \\ Y_3 &\equiv X_{n_a+1} \sim \chi^2(n - n_a - 1). \end{aligned}$$

Some calculation would reveal

$$\text{LLR}^{(1)} = -\frac{n}{2} \ln \left(1 - \frac{Y_2}{Y_2 + Y_3} \right),$$

i.e.

$$\text{LLR}^{(1)}/n \sim \mathcal{D}(n_a, n - n_a - 1).$$

To account for genotypes that do not show up in the samples, define $n_v \equiv \sum_{j \in \{j | n_j > 0\}} 1$ as the number of different genotype values across all samples. Then

$$\text{LLR}^{(1)}/n \sim \mathcal{D}(n_v - 1, n - n_v). \quad (19)$$

2. **Secondary test:** Since the null hypotheses and LLRs of primary and secondary tests are identical, $\text{LLR}^{(2)}$ follows the same null distribution as Eq 19.
3. **Independence test:** The independence test verifies if E and B are uncorrelated when conditioning on A , with $\mathcal{H}_{\text{null}}^{(3)} = E \rightarrow A \rightarrow B$. For this purpose, we keep E and A intact while randomizing \tilde{B}_i according to B 's correlation with A :

$$\tilde{B}_i \equiv \hat{\rho} A_i + \sqrt{1 - \hat{\rho}^2} X_i, \quad X_i \sim \text{i.i.d } N(0, 1).$$

Then \tilde{B}_i is normalized to B_i according to Eq 8. The null distribution of $\text{LLR}^{(3)}$ can be obtained with similar but more complex computations from Eq 6, as

$$\text{LLR}^{(3)}/n \sim \mathcal{D}(n_v - 1, n - n_v - 1). \quad (20)$$

4. **Relevance test:** The null distribution of $\text{LLR}^{(4)}$ can be obtained similarly by randomizing B_i according to Eq 7 and Eq 8, as

$$\text{LLR}^{(4)}/n \sim \mathcal{D}(n_v, n - n_v - 1).$$

5. **Controlled test:** To compute the null distribution for the controlled test, we start from

$$\tilde{B}_i = \hat{\nu}_{E_i} + \hat{\sigma}_B X_i, \quad X_i \sim N(0, 1), \quad (21)$$

and then normalize \tilde{B}_i into B_i according to Eq 8. Some calculation reveals the null distribution as

$$\text{LLR}^{(5)}/n \sim \mathcal{D}(1, n - n_v - 1).$$

We verified our analytical method of deriving null distributions by comparing the analytical null distribution v.s. null distribution from permutation for the relevance test in Section S2.2.

2.5 Bayesian inference of posterior probabilities

After obtaining the PDFs for the LLRs from real data and the null hypotheses, we can convert LLR values into posterior probabilities $P(\mathcal{H}_{\text{alt}} \mid \text{LLR})$. We use a similar technique as in [8], which itself was based on a more general framework to estimate FDRs in genome-wide studies [37]. This framework assumes that the real distribution of a certain test statistic forms a mixture distribution of null and alternative hypotheses. After estimating the null distribution, either analytically or by simulation, it can be compared against the real distribution to determine the proportion of null hypotheses, and consequently the posterior probability that the alternative hypothesis is true at any value of the statistic.

To be precise, consider an arbitrary LRT. The fundamental assumption is that in the limit $\text{LLR} \rightarrow 0^+$, all test cases come from the null hypothesis ($\mathcal{H}_{\text{null}}$), whilst as LLR increases, the proportion of alternative hypotheses (\mathcal{H}_{alt}) also grows. The mixture distribution of real LLR values is assumed to have a PDF as

$$p(\text{LLR}) = P(\mathcal{H}_{\text{null}})p(\text{LLR} \mid \mathcal{H}_{\text{null}}) + P(\mathcal{H}_{\text{alt}})p(\text{LLR} \mid \mathcal{H}_{\text{alt}}).$$

The priors $P(\mathcal{H}_{\text{null}})$ and $P(\mathcal{H}_{\text{alt}})$ sum to unity and correspond to the proportions of null and alternative hypotheses in the mixture distribution. For any test $i = 0, \dots, 5$, Bayes' theorem then yields its posterior probability as

$$P(\mathcal{H}_{\text{alt}}^{(i)} \mid \text{LLR}^{(i)}) = \frac{p(\text{LLR}^{(i)} \mid \mathcal{H}_{\text{alt}}^{(i)})}{p(\text{LLR}^{(i)})} P(\mathcal{H}_{\text{alt}}^{(i)}). \quad (22)$$

Based on this, we can define the posterior probabilities of the selected hypotheses according to Table 1, i.e. the alternative for tests 0, 1, 2, 4, 5 and the null for test 3 as

$$P_i \equiv \begin{cases} P(\mathcal{H}_{\text{alt}}^{(i)} \mid \text{LLR}^{(i)}), & i = 0, 1, 2, 4, 5, \\ P(\mathcal{H}_{\text{null}}^{(i)} \mid \text{LLR}^{(i)}), & i = 3. \end{cases} \quad (23)$$

After obtaining the LLR distribution of the null hypothesis [$p(\text{LLR} \mid \mathcal{H}_{\text{null}})$], we can determine its proportion [$P(\mathcal{H}_{\text{null}})$] by aligning $p(\text{LLR} \mid \mathcal{H}_{\text{null}})$ with the real distribution $p(\text{LLR})$ at the $\text{LLR} \rightarrow 0^+$ side. This provides all the prerequisites to perform Bayesian inference and obtain any P_i from Eq 23.

In practice, PDFs are approximated with histograms. This requires proper choices of histogram bin widths, $P(\mathcal{H}_{\text{null}})$, and techniques to ensure the conversion from LLR to posterior probability is monotonically increasing and smooth. Implementation details can be found in Findr package and in Section S1.1. Distributions can be estimated either separately for every (E, A) pair or by pooling across all (E, A) pairs. In practice, we test on the order of 10^3 to 10^4 candidate targets (“ B ”) for every (E, A) such that a separate conversion of LLR values to posterior probabilities is both feasible and recommended, as it accounts for different roles of every gene, especially hub genes, through different rates of alternative hypotheses.

Lastly, in a typical application of Findr, inputs of (E, A) pairs will have been pre-determined as the set of significant eQTL-gene pairs from a genome-wide eQTL association analysis. In such cases, we may naturally assume $P_1 = 1$ for all considered pairs, and skip the primary test.

2.6 Tests to evaluate

Based on the six tests in Section 2.3, we use the following tests and test combinations for the inference of genetic regulations, and evaluate them in the results.

- The correlation test is introduced as a benchmark, against which we can compare other methods involving genotype information. Pairwise correlation is a simple measure for the probability of two genes being functionally related either through direct or indirect regulation, or through coregulation by a third factor. Bayesian inference additionally considers different gene roles. Its predicted posterior probability for regulation is P_0 .
- The traditional causal inference test, as explained in [8], suggested that the regulatory relation $E \rightarrow A \rightarrow B$ can be confirmed with the combination of three separate tests: E regulates A , E regulates B , and E only regulates B through A (i.e. E and B become independent when conditioning on A). They correspond to the primary, secondary, and independence tests respectively. The regulatory relation $E \rightarrow A \rightarrow B$ is regarded positive only when all three tests return positive. So its probability can be broken down as

$$P_T \equiv P_1 P_2 P_3. \quad (24)$$

Trigger [38] is an R package implementation of the method. However, since Trigger integrates eQTL discovery with causal inference, it is not practical for use on modern datasets. For this reason, we reimplemented this method in Findr, and evaluated it with P_2 and $P_2 P_3$ separately, in order to assess the individual effects of secondary and independence tests. As discussed above, we expect a set of significant eQTLs and their associated genes as input, and therefore $P_1 = 1$ is assured and not calculated in this paper or the package Findr. Note that P_T is the posterior true positive rate (TPR), i.e. the probability that tests 2 and 3 are both true. Correspondingly, its FPR (the probability that one of them is false) is $1 - P_T$.

- The novel test, aimed specifically at addressing the failures of the traditional causal inference test, combines the tests differently:

$$P \equiv \frac{1}{2}(P_4 + P_2 P_5). \quad (25)$$

When the signal level is too weak for tests 2 and 5, we expect P_4 to still provide distinguishing power better than random predictions. When the interaction is strong, $P_2 P_5$ is then able to pick up true targets regardless of the existence of hidden confounders.

2.7 Evaluation methods

Given the predicted posterior probabilities for every pair (A, B) from any test, or more generically a score from any inference method, we evaluated the predictions against ground-truth tables with the metrics of Receiver Operating Characteristic (ROC) and Precision-Recall (PR) curves, as well as the Areas Under the ROC (AUROC) and Precision-Recall (AUPR) curves. In particular, AUPR is calculated with the Davis-Goadrich nonlinear interpolation [39] with R package *PRROC*.

In order to assess the effect of sample size on the performances of inference methods, we performed subsampling evaluations. This is made practically possible by the DREAM datasets which contain 999 samples with sufficient variance, as well as the computational efficiency from Findr which makes subsampling computationally feasible. With a given dataset and ground-truth table, the total number of samples n , and the number of samples of our actual interest $N < n$, we performed subsampling by repeating following steps k times:

1. Randomly select N samples out of the total n samples without replacement.
2. Infer regulations only based on the selected samples.
3. Compute and record the evaluation metrics of interest (e.g. AUROC and AUPR) with the inference results and ground-truths.

Evaluation metrics are recorded in every loop, and their means, standard deviations, and standard errors over the k runs, are calculated. The mean indicates how the inference method performs on the metric in average, while the standard deviation reflects how every individual subsampling deviates from the average performance.

3 Results

3.1 Traditional causal inference fails in the presence of hidden confounders and weak regulations

We developed a highly efficient software package Findr for causal inference of gene regulatory interactions from genome-transcriptome variation data by combining existing and novel likelihood ratio tests for various possible associations between eQTLs and pairs of gene expression traits (Section 2.3). To systematically evaluate the ability of traditional causal inference methods based on conditional independence tests (Section 2.6) to recover known regulatory interactions, we obtained five datasets with 999 samples simulated from known (synthetic) gene regulatory networks with 1,000 genes each from the DREAM5 Systems Genetics Challenge [20]. We subsampled each dataset into datasets with different sample sizes to observe how performance is affected by sample size (see Section 2.7 for details). We demonstrate representative results from the fourth dataset here, whilst others are included in the supplementary material (Section S2.3).

The traditional method combines the secondary (P_2) and independence (P_3) tests sequentially (Section 2.6). To disentangle the effects of each test, we compared the performances of P_2 and P_2P_3 separately against the benchmark correlation test (P_0) in terms of AUROC and AUPR. Both the secondary test alone and the traditional causal inference test combination were shown to *underperform* correlation test (Figure 1). Moreover, the inclusion of the conditional independence test *worsens* inference accuracy, more so with increasing sample size (Figure 1) and increasing number of regulations per gene (Section S2.3). The performance drop with increasing sample size is also observed using CIT [13], based on its predictions on all 15 DREAM datasets (Figure S3). CIT is an R package that includes the conditional independence test, along with tests 2 and 5, while also comparing $E \rightarrow A \rightarrow B$ against $E \rightarrow B \rightarrow A$. The subsampling analysis on CIT was not feasible due to its lack of speed.

We identified two causes why traditional causal inference did not work as expected. First, the secondary test underperforms the correlation test due to a lower power for distinguishing weak interactions. In a true regulation $E \rightarrow A \rightarrow B$, the secondary linkage ($E \rightarrow B$) is the result of two direct linkages ($E \rightarrow A$ and $A \rightarrow B$) chained together, and is harder to identify than either of them. This hinders the secondary test’s ability to identify some of the true causal interactions that are picked up by the correlation test, and substantially raises its *false negative rate* (FNR). Secondly, hidden confounders cause the counter-productive influence of the conditional independence test. As understood in [8] and shown in Figure 2, even if $E \rightarrow A \rightarrow B$ is genuine, the conditional independence test will find E and B to be still correlated after conditioning on A in the presence of confounders. Therefore the conditional independence test will only report positive on $E \rightarrow A \rightarrow B$ relations without any confounders, thus further raising the false negative rate. This is supported by multiple observations:

- When the number of regulations per gene is smaller (i.e. with smaller DREAM dataset numbering), the conditional independence test causes fewer false negatives and therefore has better performance (Figure S2).
- The residual correlation between E and B after conditioning on A in the presence of a hidden confounder C requires three chained regulations $E \rightarrow A$, $C \rightarrow A$, and $C \rightarrow B$. This indirect effect tends to be weaker and consequently starts to show up on larger sample sizes than direct effects (e.g. correlation test) or indirect two-chained effects (e.g. secondary test). This indicates that in a subsampling evaluation from the same dataset, the conditional independence test may demonstrate a productive net effect at small sample sizes, but a counter-productive net effect at large sample sizes.

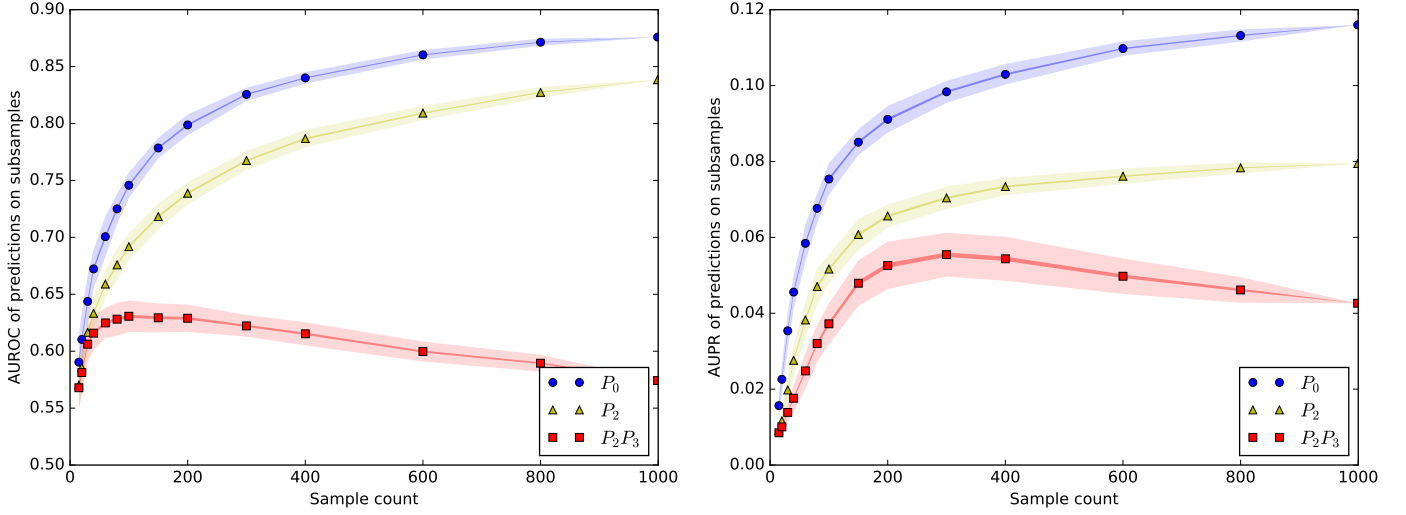


Figure 1: The mean AUROC and AUPR on subsampled data are shown for traditional causal inference test against the baseline correlation test, both implemented in Findr. Every marker corresponds to the average AUROC or AUPR at specific sample sizes. Subsampling at every sample size were performed 100 times. Half widths of the lines and shades are the standard errors and standard deviations respectively, of AUROC or AUPR. This result is for dataset 4 of DREAM. For results on other datasets, see Figure S2.

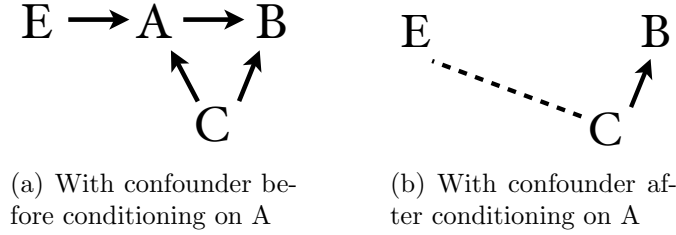


Figure 2: The conditional independence test fails in the presence of confounders. When A and B are both regulated by a confounder C , which is independent of E (Figure 2(a)), conditioning on A would introduce inter-dependency between E and C , which maintains $E \rightarrow B$ regulation (Figure 2(b)).

- CIT shows a similar performance drop pattern with increasing sample size. CIT is an R package developed independently from this paper (or the authors), but also utilizes the conditional independence test.

Given the above observations, the traditional causal inference test failed to make use of genotype information and did not deliver better performance than using expression correlation alone. This is due to two pitfalls in dealing with weak regulations and hidden confounders, both of which incurred an elevated false negative rate.

3.2 Findr accounts for weak secondary linkage and hidden confounders and outperforms existing methods on simulated data

To overcome the limitations of traditional causal inference methods, we introduced two additional tests (Section 2.3 and Table 1). The relevance test (P_4) verifies that B is not independent from A and E simultaneously and is more sensitive for picking up weak secondary linkages than the secondary linkage test. The controlled test (P_5) excludes that E is pleiotropic for A and B , ensuring that the correlation between A and B cannot be fully explained by E .

The same subsampling analysis as before revealed that P_4 performed best in terms of AUROC, and AUPR with small sample sizes, whilst the combination P_2P_5 achieved highest AUPR for larger sample sizes (Figure 3). Most importantly, both tests consistently outperformed the correlation test

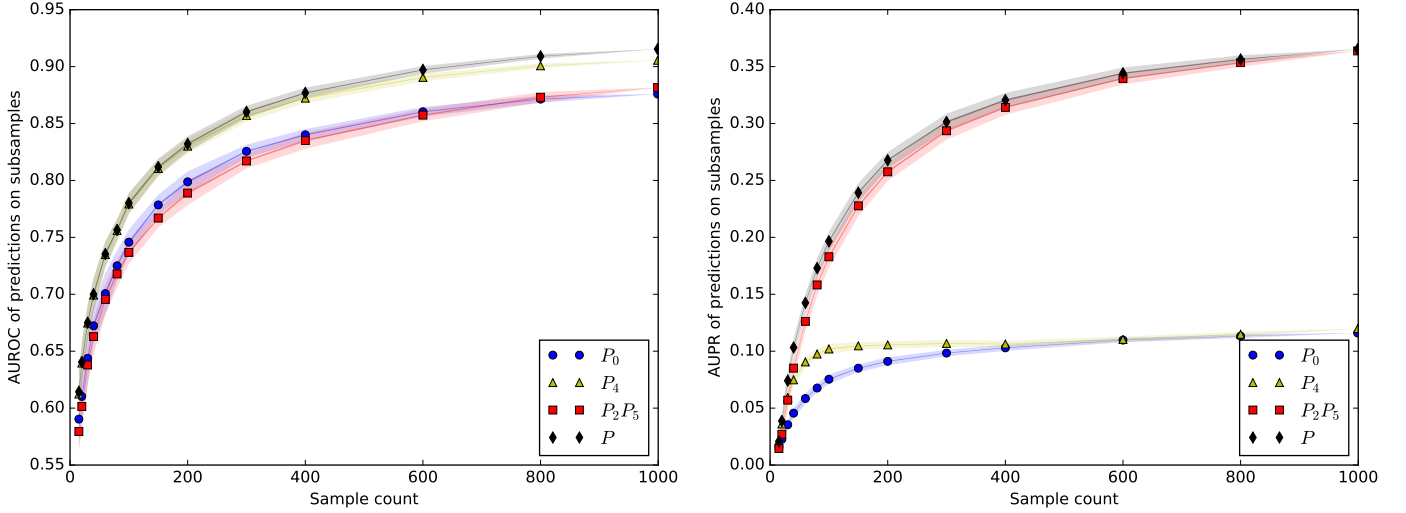


Figure 3: The mean AUROC and AUPR on subsampled data are plotted for newly proposed tests against the baseline correlation test. Every marker corresponds to the average AUROC or AUPR at specific sample sizes. Subsampling at every sample size were performed 100 times. Half widths of the lines and shades are the standard errors and standard deviations respectively, of AUROC or AUPR. P is the new composite test defined in Eq 25, which achieved better performance than either individual test. This result is for dataset 4 of DREAM. For results on other datasets, see Figure S4.

(P_0), particularly for AUPR. This demonstrates conclusively that the inclusion of genotype data can improve regulatory network inference. These observations are consistent across all five DREAM datasets (Figure S4). To combine the relative advantages of P_4 and P_2P_5 , we constructed a composite test (P) as the average of the two probabilities (cf. Eq 25), which outperformed P_4 and P_2P_5 at all sample sizes and hence is our recommended new test for causal inference.

As a final evaluation on DREAM data, we compared the performances of Findr’s new test (P), Findr’s correlation test (P_0), Findr’s traditional causal inference test (P_T), and CIT on all 15 datasets against the published leaderboard of the DREAM5 Systems Genetics Challenge [20]. Findr’s new test achieved highest AUROC and highest AUPR on all 15 datasets (Table S1). It is important to note that best performers can differ on different datasets or on AUROC and AUPR. For instance, the challenge winner [40] attained best AUROC on 6/15 datasets and best AUPR on 5. When compared to other inference methods that also reported improvements [41–43], Findr demonstrates additional virtues besides the inference accuracy. Its nonparametric nature ensures robust performances across datasets without parameter tuning. Its pairwise computation scales linearly in time with the number of regulators, targets, and samples, as opposed to multivariate regression methods, providing scalability to datasets that are orders of magnitude larger.

3.3 Findr outperforms multivariate machine learning methods on microRNA target prediction in human lymphoblastoid cells

To evaluate Findr on a real dataset, we performed causal inference on mRNA and microRNA sequencing data in lymphoblastoid cell lines from 360 European individuals in the Geuvadis study [14]. We first considered 55 miRNAs that were reported to have a significant cis-eQTL at an FDR threshold of 5%, against 23,722 genes. MicroRNAs are small endogenous regulatory RNAs which are incorporated into an RNA induced silencing complex (RISC) that binds to sites of variable complementarity in target messenger RNAs, triggering their degradation and/or repressing their translation [44]. Since miRNA target predictions from sequence complementarity alone result in high numbers of false positives, prediction methods based on correlating miRNA and gene expression profiles are of great interest [45]. Although miRNA target prediction using causal inference from genotype and gene expression data has been considered in mouse [46], it remains unknown whether the inclusion of genotype

data improves existing expression-based methods.

To facilitate unbiased comparison of target prediction methods, the miRLAB resource has recently been created, consisting of a reference network of miRNA-gene regulatory interactions combining the most commonly used databases of experimentally confirmed miRNA target genes, and a uniform interface to predict miRNA targets from expression data using twelve prediction methods including linear and non-linear, pairwise and multivariate regression methods [24].

We were able to infer miRNA targets with 11/12 miRLAB methods, the GENIE3 random forest regression method [47], CIT, and the three tests in Findr: the traditional causal inference (P_T), new (P), and correlation (P_0) tests. Comparison between the 16 methods demonstrated consistency with the evaluation on simulated DREAM data (Section 3.2). Findr’s new test achieved higher AUROC and AUPR than all other methods attempted, while also being over 500 (Findr’s correlation test against Pearson correlation) to over 500,000 (Findr’s new causal inference against CIT) times faster (Table S2). The full ROC and PR curves can be found in Figure S5.

3.4 Findr accurately predicts transcription factor targets in human lymphoblastoid cells

Next we considered 3,172 genes with significant cis-eQTLs at 5% FDR threshold [14] and again applied Findr to infer regulatory interactions to the 23,722 target genes for the traditional (P_T), new (P) and correlation (P_0) tests. Groundtruths of experimentally confirmed causal gene interactions in human, and mammalian systems more generally, are of limited availability and mainly concern transcription or transcription-associated DNA-binding factors (TFs). Here we focused on a set of 25 TFs in the set of eQTL-genes for which either differential expression data following siRNA silencing (6 TFs) or TF-binding data inferred from ChIP-sequencing and/or DNase footprinting (20 TFs) in a lymphoblastoid cell line (GM12878) was available [21] (see Section 2.1 for details).

As shown in Figure S6, AUPRs and AUROCs did not exhibit substantial differences, other than modest improvement over random predictions. We believe this is due to the unavoidable noise and size limitations in groundtruth data, which lead to large fluctuations in evaluation metrics and therefore cannot compare methods perfectly. Furthermore, the AUPR and AUROC test the entire ranked list of predictions for overlap with the groundtruth and will miss differences in enrichment for true positives between methods if they occur only among a small fraction of top-ranked predictions. We therefore took advantage of the fact that Findr’s probabilities are true positive rate estimates for each test in Table 1. Hence we assessed how estimated TPRs of traditional, new, and correlation tests reflect the actual TPR at thresholds ranging from 0.1 to 0.9 in Figure 4. Findr’s new test correctly reflected the estimated TPR values at various threshold levels, and was able to identify true regulations at high TPR control levels. However, the traditional test significantly underestimated TPRs due to its elevated FNR by design (Section 3.1). This led to its lack of positive predictions at high estimated TPR thresholds and enrichment of true regulations at low thresholds, essentially nullifying the TPR meaning of its output probability P_T . On the other hand, the correlation test significantly overestimated TPRs simply because it is unable to distinguish causal, reversed causal or confounded interactions, which raised its FPR.

The construction of gold standard regulatory networks from TF-binding data is dependent on how TF binding sites are mapped to target genes. Here a TF regulatory interaction was assumed if a gene had at least two binding sites for a particular TF within 10kb of its transcription start site (TSS) [21]. We repeated the analysis using the high-confidence (binding within 2.5kb) TF-target network derived from ENCODE from ChIP-sequencing data of 119 TFs in five cell types, including the lymphoblastoid cell line GM12878 [23]. Fourteen TFs had a significant eQTL in the Geuvadis data. The analysis results are consistent (Figure S6 and Figure S7).

4 Discussion

Rapid advances in sequencing technology have made it possible to generate genome and transcriptome variation data in diverse cell types, tissues and organs across hundreds of individuals, and thereby

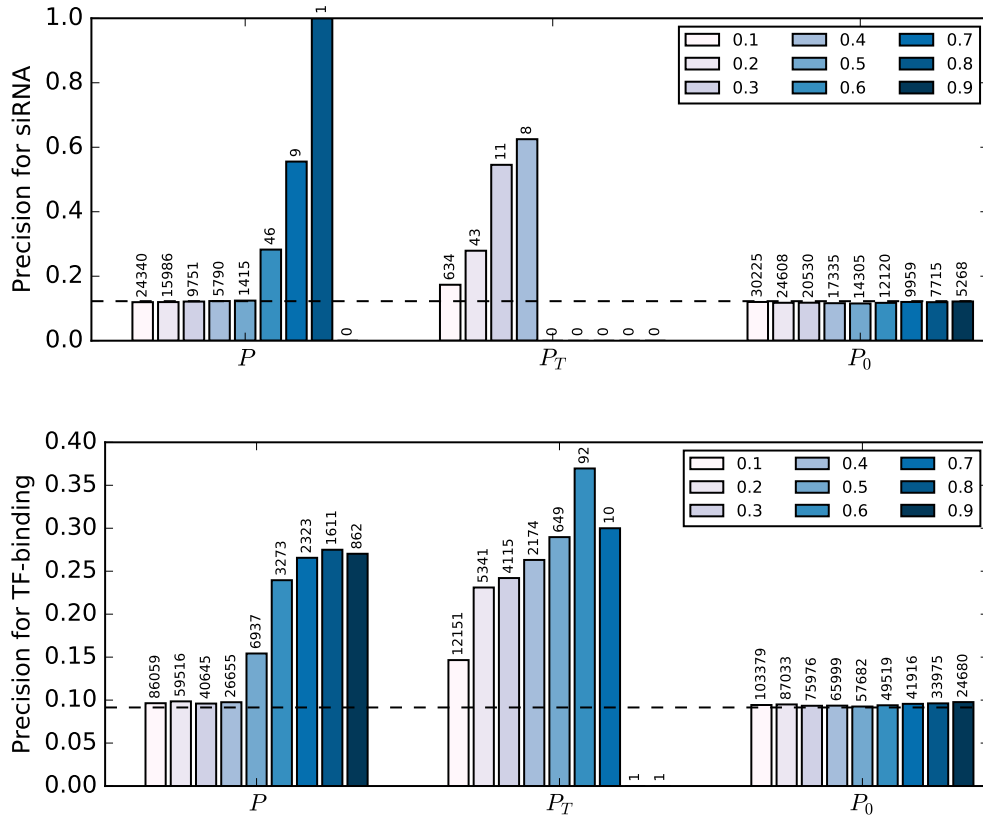


Figure 4: Inference precision at probability cutoffs 0.1 to 0.9 (light to dark) with respect to groundtruth networks derived from siRNA silencing of 6 TFs (top) and TF-binding of 20 TFs (bottom). The number above each bar indicates the number of positive predictions at the corresponding threshold. The dashed line is precision from random predictions.

allow to study the impact of genetic variation on complex human diseases and quantitative traits in exquisite detail. It has been known that by using genetic variation at eQTLs as a causal anchor or instrumental variable, causality between two genes can be inferred through a conditional independence test, provided they have no common upstream regulators (hidden confounders). However this assumption is at odds with the fact that genes are organized in complex hierarchical gene regulatory networks where common regulation of regulator-target pairs is an abundant feature. On the other hand, since no previous causal inference software has been able to handle the size of modern datasets, the extent to which integration of genome and transcriptome variation data can inform the inference of causal gene networks has remained elusive.

Here we developed a highly efficient software package Findr (Fast Inference of Networks from Directed Regulations) implementing novel and existing causal inference tests. Application of Findr on hundreds of datasets simulated from synthetic gene networks with known genetic architecture showed that our novel tests, which account for weak secondary linkage and hidden confounders, resulted in a significantly improved overall performance on every single dataset tested. Proving in an easily reproducible manner that these results also hold on human data is challenging, due to the often restricted access to individual-level genotype data and the limited availability of reference databases of known interactions, especially when cell type specificity is taken into account. We performed our evaluation on the Geuvadis data, which provides transcriptome data in lymphoblastoid cells of nearly 400 individuals whose genotype data is publicly available through the 1000 Genomes project. We found that Findr more accurately predicts miRNA targets compared to other causal inference methods and a panel of machine learning methods that used expression data alone. Although the absolute power to predict miRNA targets may appear modest (area under the ROC curve ~ 0.6), we were primarily interested in the relative performance of various methods, and did not incorporate information about known miRNA biology, such as a preference for negative correlations or the presence of miRNA seed sequences. Moreover, since miRNAs are frequently studied in the context of diseases such as cancer, the ground-truth set of experimentally confirmed targets may represent a biased set of interactions that are not necessarily present in the current cell type studied.

To address the issue of cell type specificity, we analysed the predicted targets of 25 transcription factors for which either functional targets from siRNA silencing experiments or DNA-binding targets from ChIP-sequencing or DNase footprinting in lymphoblastoid cells were available. For both data types we found that Findr achieved a 2 to 5-fold enrichment for known TF targets compared to using TF-target coexpression alone. The Findr predictions formed a subset of the coexpression edges at the same FPR threshold, showing that causal inference is indeed able to prioritize highly probable causal interactions among coexpressed genes. Although Findr and conditional-independence based causal inference resulted in similar performances in this case, the estimated FPR values of the traditional method were greatly inflated, such that enrichment for known interactions was only observed at FPRs of 50-80%. This reaffirms the finding, consistently observed in all our analyses, that the conditional-independence method is over conservative for calling causal interactions in the context of complex regulatory networks.

It is worth noting that among all six likelihood ratio tests, given the eQTL variable, only the conditional independence test is asymmetric between the two genes considered, but was excluded due to poor performance. Hence in Findr, the direction of causality arises predominantly from using a different eQTL when testing the reverse interaction. In the context of gene regulation, cis-regulatory eQTLs are presumed to lie close to their target genes on the genome, and thus the vast majority of coexpressed gene pairs will indeed have different causal anchor eQTLs. In the few cases where coexpressed and typically duplicated genes are colocated on the genome, the only information to determine the causal direction is the strength of the primary linkage test. However in these cases it is likely that the shared eQTL regulates the genes independently, and this is accounted for by the ‘controlled’ test.

In this paper we have addressed the challenge of pairwise causal inference, but to reconstruct the actual pathways and networks that affect a phenotypic trait, two important limitations have to be considered. First, linear pathways propagate causality, and may thus appear as densely connected sets of triangles in pairwise causal networks. Secondly, most genes are regulated by multiple upstream fac-

tors, and hence some true edges will only have a small posterior probability unless they are considered in an appropriate multivariate context. The most straightforward way to address these issues would be to model the real directed interaction network as a Bayesian network with sparsity constraints. A major advantage of Findr is that it outputs easily interpretable and parameter-free probability values which can be directly incorporated as prior edge probabilities in existing network inference softwares.

In summary, the development of Findr provides the community for the first time with a highly efficient and accurate open source software tool for causal inference from large-scale genome-transcriptome variation data which paves the way for future multivariate network modelling efforts.

Funding

This work has been supported by the BBSRC (grant numbers BB/J004235/1 and BB/M020053/1).

References

- [1] N Friedman. Inferring cellular networks using probabilistic graphical models. *Science*, 308:799–805, 2004.
- [2] M Bansal, V Belcastro, A Ambesi-Impiombato, and D di Bernardo. How to infer gene networks from expression profiles. *Mol Syst Biol*, 3:78, 2007.
- [3] Frank Emmert-Streib, Galina Glazko, Ricardo De Matos Simoes, et al. Statistical inference and reverse engineering of gene regulatory networks from observational expression data. *Frontiers in Genetics*, 3:8, 2012.
- [4] Frank W Albert and Leonid Kruglyak. The role of regulatory variation in complex traits and disease. *Nature Reviews Genetics*, 16:197–212, 2015.
- [5] Matthew V Rockman. Reverse engineering the genotype–phenotype map with natural genetic variation. *Nature*, 456(7223):738–744, 2008.
- [6] Yang Li, Bruno M Tesson, Gary A Churchill, and Ritsert C Jansen. Critical reasoning on causal inference in genome-wide linkage and association studies. *Trends in Genetics*, 26(12):493–498, 2010.
- [7] J Zhu, P Y Lum, J Lamb, D GuhaThakurta, S W Edwards, R Thieringer, J P Berger, M S Wu, J Thompson, A B Sachs, and E E Schadt. An integrative genomics approach to the reconstruction of gene networks in segregating populations. *Cytogenet Genome Res*, 105:363–374, 2004.
- [8] Lin Chen, Frank Emmert-Streib, and John Storey. Harnessing naturally randomized transcription to infer regulatory relationships among genes. *Genome Biology*, 8(10):R219, 2007.
- [9] Jason E Aten, Tova F Fuller, Aldons J Lusis, and Steve Horvath. Using genetic markers to orient the edges in quantitative trait networks: the NEO software. *BMC Systems Biology*, 2(1):34, 2008.
- [10] Eric E Schadt, John Lamb, Xia Yang, Jun Zhu, Steve Edwards, Debraj GuhaThakurta, Solveig K Sieberts, Stephanie Monks, Marc Reitman, Chunsheng Zhang, et al. An integrative genomics approach to infer causal associations between gene expression and disease. *Nature Genetics*, 37(7):710–717, 2005.
- [11] Elias Chaibub Neto, Christine T Ferrara, Alan D Attie, and Brian S Yandell. Inferring causal phenotype networks from segregating populations. *Genetics*, 179(2):1089–1100, 2008.
- [12] Elias Chaibub Neto, Aimee T Broman, Mark P Keller, Alan D Attie, Bin Zhang, Jun Zhu, and Brian S Yandell. Modeling causality for pairs of phenotypes in system genetics. *Genetics*, 193(3):1003–1013, 2013.
- [13] Joshua Millstein, Bin Zhang, Jun Zhu, and Eric E. Schadt. Disentangling molecular relationships with a causal inference test. *BMC Genetics*, 10(1):1–15, 2009.

- [14] Tuuli Lappalainen, Michael Sammeth, Marc R. Friedlander, Peter A. C. /t Hoen, Jean Monlong, Manuel A. Rivas, Mar Gonzalez-Porta, Natalja Kurbatova, Thasso Griebel, Pedro G. Ferreira, Matthias Barann, Thomas Wieland, Liliana Greger, Maarten van Iterson, Jonas Almlöf, Paolo Ribeca, Irina Pulyakhina, Daniela Esser, Thomas Giger, Andrew Tikhonov, Marc Sultan, Gabrielle Bertier, Daniel G. MacArthur, Monkol Lek, Esther Lizano, Henk P. J. Buermans, Ismael Padiou, Thomas Schwarzmayer, Olof Karlberg, Halit Ongen, Helena Kilpinen, Sergi Beltran, Marta Gut, Katja Kahlem, Vyacheslav Amstislavskiy, Oliver Stegle, Matti Pirinen, Stephen B. Montgomery, Peter Donnelly, Mark I. McCarthy, Paul Flicek, Tim M. Strom, The Geuvadis Consortium, Hans Lehrach, Stefan Schreiber, Ralf Sudbrak, Angel Carracedo, Stylianos E. Antonarakis, Robert Hasler, Ann-Christine Syvanen, Gert-Jan van Ommen, Alvis Brazma, Thomas Meitinger, Philip Rosenstiel, Roderic Guigo, Ivo G. Gut, Xavier Estivill, and Emmanouil T. Dermitzakis. Transcriptome and genome sequencing uncovers functional variation in humans. *Nature*, 501(7468):506–511, 09 2013.
- [15] Benjamin P Fairfax, Peter Humburg, Seiko Makino, Vivek Naranbhai, Daniel Wong, Evelyn Lau, Luke Jostins, Katharine Plant, Robert Andrews, Chris McGee, and Julian C Knight. Innate immune activity conditions the effect of regulatory variants upon monocyte gene expression. *Science*, 343(6175):1246949, 2014.
- [16] Kristin G Ardlie, David S Deluca, Ayellet V Segrè, Timothy J Sullivan, Taylor R Young, Ellen T Gelfand, Casandra A Trowbridge, Julian B Maller, Taru Tukiainen, Monkol Lek, et al. The genotype-tissue expression (GTEx) pilot analysis: Multitissue gene regulation in humans. *Science*, 348(6235):648–660, 2015.
- [17] O. Franzén, R. Ermel, A. Cohain, N. Akers, A. Di Narzo, H. Talukdar, H. Foroughi Asl, C. Giambartolomei, J. Fullard, K. Sukhvasi, S. Köks, L.-M. Gan, C. Giannarelli, J. Kovacic, C. Betsholtz, B. Losic, T. Michoel, K. Hao, P. Roussos, J. Skogsberg, A. Ruusalepp, E. Schadt, and J. Björkegren. Cardiometabolic risk loci share downstream cis-and trans-gene regulation across tissues and diseases. *Science*, 353:827–830, 2016.
- [18] A. Gitter, Z. Siegfried, M. Klutstein, O. Fornes, B. Oliva, I. Simon, and Z. Bar-Joseph. Backup in gene regulatory networks explains differences between binding and knockout results. *Mol Syst Biol*, 5(1), 2009.
- [19] U Alon. Network motifs: theory and experimental approaches. *Nat Rev Genet*, 8:450–461, 2007.
- [20] DREAM5 Systems Genetics challenges, <https://www.synapse.org/#!/Synapse:syn2820440/wiki/>, 2014.
- [21] Darren A Cusanovich, Bryan Pavlovic, Jonathan K Pritchard, and Yoav Gilad. The functional consequences of variation in transcription factor binding. *PLoS Genetics*, 10(3):e1004226, 2014.
- [22] Roger Pique-Regi, Jacob F Degner, Athma A Pai, Daniel J Gaffney, Yoav Gilad, and Jonathan K Pritchard. Accurate inference of transcription factor binding from DNA sequence and chromatin accessibility data. *Genome research*, 21(3):447–455, 2011.
- [23] M.B. Gerstein, A. Kundaje, M. Hariharan, S.G. Landt, K.K. Yan, C. Cheng, X.J. Mu, E. Khurana, J. Rozowsky, R. Alexander, et al. Architecture of the human regulatory network derived from ENCODE data. *Nature*, 489(7414):91–100, 2012.
- [24] Thuc Duy Le, Junpeng Zhang, Lin Liu, Huawen Liu, and Jiuyong Li. mirlab: An r based dry lab for exploring mirna-mrna regulatory relationships. *PLoS ONE*, 10(12):1–15, 12 2015.
- [25] Andrea Pinna, Nicola Soranzo, Ina Hoeschele, and Alberto de la Fuente. Simulating systems genetics data with sysgensim. *Bioinformatics*, 27(17):2459–2462, 2011.
- [26] Jianlong Qi, Hassan Foroughi Asl, Johan Björkegren, and Tom Michoel. krux: matrix-based non-parametric eqtl discovery. *BMC Bioinformatics*, 15(1):11, 2014.
- [27] Geuvadis genotype data, <ftp://ftp.ebi.ac.uk/pub/databases/microarray/data/experiment/GEUV/E-GEUV-1/genotypes/>, 2013.

- [28] Geuvadis gene expression data, ftp://ftp.ebi.ac.uk/pub/databases/microarray/data/experiment/GEUV/E-GEUV-1/analysis_results/GD462.GeneQuantRPKM.50FN.samplename.resk10.txt.gz, 2013.
- [29] Geuvadis miRNA expression data, ftp://ftp.ebi.ac.uk/pub/databases/microarray/data/experiment/GEUV/E-GEUV-2/analysis_results/GD452.MirnaQuantCount.1.2N.50FN.samplename.resk10.txt, 2013.
- [30] Geuvadis best eQTL data, ftp://ftp.ebi.ac.uk/pub/databases/microarray/data/experiment/GEUV/E-GEUV-2/analysis_results/EUR363.mi.cis.FDR5.best.rs137.txt.gz, 2013.
- [31] miRLAB ‘strong’ ground-truth data, https://downloads.sourceforge.net/project/mirlab/groundtruth_Strong, 2015.
- [32] Thanasis Vergoulis, Ioannis S. Vlachos, Panagiotis Alexiou, George Georgakilas, Manolis Maragkakis, Martin Reczko, Stefanos Gerangelos, Nectarios Koziris, Theodore Dalamagas, and Artemis G. Hatzigeorgiou. Tarbase 6.0: capturing the exponential growth of mirna targets with experimental support. *Nucleic Acids Research*, 40(D1):D222–D229, 2012.
- [33] Feifei Xiao, Zhixiang Zuo, Guoshuai Cai, Shuli Kang, Xiaolian Gao, and Tongbin Li. mirecords: an integrated resource for microrna–target interactions. *Nucleic Acids Research*, 37(suppl 1):D105–D110, 2009.
- [34] Harsh Dweep, Carsten Sticht, Priyanka Pandey, and Norbert Gretz. mirwalk - database: Prediction of possible mirna binding sites by walking the genes of three genomes. *Journal of Biomedical Informatics*, 44(5):839–847, 2011.
- [35] Sheng-Da Hsu, Yu-Ting Tseng, Sirjana Shrestha, Yu-Ling Lin, Anas Khaleel, Chih-Hung Chou, Chao-Fang Chu, Hsi-Yuan Huang, Ching-Min Lin, Shu-Yi Ho, Ting-Yan Jian, Feng-Mao Lin, Tzu-Hao Chang, Shun-Long Weng, Kuang-Wen Liao, I-En Liao, Chun-Chi Liu, and Hsien-Da Huang. mirtarbase update 2014: an information resource for experimentally validated mirna–target interactions. *Nucleic Acids Research*, 42(D1):D78–D85, 2014.
- [36] Andrey A. Shabalin. Matrix eqtl: ultra fast eqtl analysis via large matrix operations. *Bioinformatics*, 28(10):1353–1358, 2012.
- [37] John D. Storey and Robert Tibshirani. Statistical significance for genomewide studies. *Proceedings of the National Academy of Sciences*, 100(16):9440–9445, 2003.
- [38] Lin S. Chen, Dipen P. Sangurdekar, and John D. Storey. *trigger: Transcriptional Regulatory Inference from Genetics of Gene Expression*, 2007. R package version 1.16.0.
- [39] Jesse Davis and Mark Goadrich. The relationship between precision-recall and roc curves. In *Proceedings of the 23rd International Conference on Machine Learning, ICML ’06*, pages 233–240, New York, NY, USA, 2006. ACM.
- [40] Matthieu Vignes, Jimmy Vandel, David Allouche, Nidal Ramadan-Alban, Christine Cierco-Ayrolles, Thomas Schiex, Brigitte Mangin, and Simon De Givry. Gene regulatory network reconstruction using bayesian networks, the dantzig selector, the Lasso and their meta-analysis. *PloS one*, 6(12):e29165, 2011.
- [41] Marit Ackermann, Mathieu Clément-Ziza, Jacob J Michaelson, and Andreas Beyer. Teamwork: improved eQTL mapping using combinations of machine learning methods. *PloS one*, 7(7):e40916, 2012.
- [42] Robert J Flassig, Sandra Heise, Kai Sundmacher, and Steffen Klamt. An effective framework for reconstructing gene regulatory networks from genetical genomics data. *Bioinformatics*, 29(2):246–254, 2013.
- [43] Vân Anh Huynh-Thu, Louis Wehenkel, and Pierre Geurts. Gene regulatory network inference from systems genetics data using tree-based methods. *Gene Network Inference: Verification of Methods for Systems Genetics Data*, page 63, 2014.
- [44] David P Bartel. MicroRNAs: genomics, biogenesis, mechanism, and function. *Cell*, 116(2):281–297, 2004.

- [45] Jim C Huang, Tomas Babak, Timothy W Corson, Gordon Chua, Sofia Khan, Brenda L Gallie, Timothy R Hughes, Benjamin J Blencowe, Brendan J Frey, and Quaid D Morris. Using expression profiling data to identify human microRNA targets. *Nature Methods*, 4(12):1045–1049, 2007.
- [46] Wan-Lin Su, Robert R Kleinhanz, and Eric E Schadt. Characterizing the role of mirnas within gene regulatory networks using integrative genomics techniques. *Molecular Systems Biology*, 7(1):490, 2011.
- [47] Vân Anh Huynh-Thu, Alexandre Irrthum, Louis Wehenkel, and Pierre Geurts. Inferring regulatory networks from expression data using tree-based methods. *PLoS ONE*, 5(9):1–10, 09 2010.
- [48] Larry Wasserman. *All of statistics: a concise course in statistical inference*. Springer Science & Business Media, 2013.

Supplementary material for *Efficient causal inference with hidden confounders from genome-transcriptome variation data*

Lingfei Wang and Tom Michoel

Division of Genetics and Genomics, The Roslin Institute
University of Edinburgh, Easter Bush, EH25 9RG, UK

S1 Methods

S1.1 Practical details for Bayesian inference

In practice, real PDFs are approximated with histograms. This requires a proper choice of histogram bin widths and counts. We use $\lfloor n_p^{\frac{1}{2.5}} \rfloor$ bins, capped at 100, where n_p is the total number of points used for generating the histogram. The exponent is chosen for simultaneous precision improvements from higher bin resolution and weaker fluctuation within every bin. The bin widths are also chosen as a smooth transition from uniform sample count for every bin on the 0^+ side, to uniform bin width on the positive side. (See source code for detail.)

The bin values from real data were then postprocessed to remove empty bins that are between nonempty bins, by filling them with bin values on the positive side. We then aligned the analytical null histogram by intersecting it below the postprocessed real histogram at nonzero bin values. This obtained the ratio of null hypothesis in the mixture distribution. Bayes' theorem then gave raw posterior probability $P(\mathcal{H}_{\text{alt}} \mid \text{LLR})$ at every bin center.

To enforce monotonicity of posterior distribution, we calculated the two following functions. First, starting from raw posterior probability $P(\mathcal{H}_{\text{alt}} \mid \text{LLR})$ at every bin center, set every the posterior at every bin to be no smaller than every value on its the negative side. Second, also starting from raw posterior distribution values $P(\mathcal{H}_{\text{alt}} \mid \text{LLR})$ at every bin center, set every the posterior at every bin to be no larger than every value on its the positive side. A mean is then taken between the two functions to ensure monotonicity whilst minimizing systematic bias.

We then smoothened the monotonic posterior distribution, by convolving its bin differences against a predefined normal filter, after which cumulative sum was calculated to recover the posterior distribution. A normalization was then performed to maintain the span between the previous minimum and maximum. The major purpose of smoothening is to remove duplicate values, especially those introduced during monotonicity enforcement, rather than to obtain a visually smooth function. After smoothening, we performed linear interpolation to obtain the individual post-processed posterior probabilities for each LLR.

More details can be found in the source code.

S2 Results

S2.1 Iterative conditioning conflicts with FPR-based probability estimation

In [8], the authors suggested that the probability of each test should be conditioned on the survival of all preceding tests, i.e. that the null distribution of each test should be estimated only on the (A, B) pairs that survive all preceding tests, although this is not implemented in Trigger package.

As an example, we applied the test combination P_2P_3 on Geuvadis dataset. After choosing an appropriate threshold probability for secondary test, as suggested in [8], we filtered only the gene

pairs positive for secondary test and calculated their real and null LLR distributions of the independence test. Random permutations were applied for null distribution, with high-speed sampling from Metropolis-Hastings algorithm, whose sampling rate is exponentially increasing below secondary test’s positivity threshold, and uniformly 1 above that. To balance between efficient sampling and the prevention of being trapped in local maxima, a proper exponential factor of sampling rate ($\approx 1 - n_v/n$) can be obtained from the null LLR distribution in Eq 19.

The calculation revealed that the null and real distributions form different shapes at the $\text{LLR}^{(3)} \rightarrow 0^+$ side, which contradicted with the fundamental assumption of the FPR-based probability estimation method (Section 2.5). On the other hand, the histograms aligned flawlessly without conditioning. We conclude that although appropriate conditioning may enhance statistical power, we are still yet to find a self-consistent approach. Since unconditioned tests have been shown self-consistent and reliable, we do not apply test conditioning in Findr.

S2.2 Analytical null distribution matches random permutations

An important feature of Findr is the novel derivation of analytical expressions for the distributions of likelihood ratio test statistics under various null distributions (Section 2.4). We compared the analytical null distributions to empirical null distributions obtained from random simulations. Simulated data were obtained either by permuting sample labels of the independent gene (tests 0,1,2,4), or by simulating expression levels of the gene whilst taking into account existing correlations (tests 3,5). Sufficient simulated data were then fed into the original algorithm to obtain $p(\text{LLR} | \mathcal{H}_{\text{null}})$. As demonstrated with an example in Figure S1, our analytical derivation was confirmed indistinguishable with simulated distribution for miRNA hsa-miR-200b-3p’s targets.

More importantly, the analytical result holds for any sample size and does not assume infinite sample sizes ($n \rightarrow \infty$). Indeed, in this asymptotic limit, the LLRs of null distributions reduce to χ^2 distributions, in agreement with Wilks’s theorem [48]. For example, it is easy to confirm: $\lim_{n \rightarrow \infty} 2 \text{LLR}^{(1)} \sim \chi^2(n_v - 1)$. However, approximating LLR distributions with χ^2 leads to over-estimation of the null PDF at $\text{LLR} \rightarrow 0^+$ and under-estimation at $\text{LLR} \rightarrow \infty$. The tilted $p(\text{LLR} | \mathcal{H}_{\text{null}})$ would then cause systematic over-estimation of $P(\mathcal{H}_{\text{alt}} | \text{LLR})$ for all pairs. For the Geuvadis dataset with 360 samples and $n_v = 3$, an over-estimation of $\sim 1\%$ is observed at $\text{LLR} \rightarrow 0^+$. This counts an extra $\sim 1\%$ of all pairs as the alternative hypothesis, which can be of the same order as the actual percentage of true alternative hypotheses (typically at most a few percent).

S2.3 Subsampling performances of existing and new causal inference methods on DREAM datasets

DREAM challenge contains five datasets that have 999 samples. With numbering 1 to 5, they each contain different number of true regulations, from ~ 1000 to ~ 5000 incrementally, for the purpose of characterizing regulatory networks of different complexity. As mentioned in Section 3.1 and Section 3.2, performances on the fourth dataset are shown in the main article, and the rest here in Figure S2 and Figure S4.

S2.4 Findr achieves best performance on miRNA target predictions from Geuvadis dataset

We also compared the performance of Findr on miRNA target prediction from the Geuvadis dataset with a suite of network inference methods that are based on gene expression data and, for some, genotype information. They include:

- All methods in the miRLAB package [24]:
 - **Correlation methods:** Pearson correlation, Spearman correlation, Kendal correlation, Distance correlation (dcov), Hoeffding’s D measure (hoeffding), Randomized Dependence Coefficient (rdc), and Mutual Information (mi).

- **Regression methods:** Lasso, and Elastic-net (elastic).
- **Other methods:** Z-score, and Roleswitch (promise).
- **Failed method:** Intervention calculus (ida) method failed due to excessive memory usage (greater than 16GB) and hence is excluded from comparison.
- GENIE3 [47] which utilizes random forests.
- CIT [13] which performs multiple causal inference tests with genotype data.
- Multiple tests implemented in Findr, including: traditional (P_T), new (P), and correlation (P_0) tests.

The Trigger package was not attempted because its eQTLs discovery routine exceeds both our memory and time limitations.

Their AUROCs, AUPRs, and running times are presented in Table S2. The ROC and PR curves are shown in Figure S5. We observed the following results:

- The correlation test topped among methods without genotype information, and in particular performs much better than Pearson and Spearman correlations. The performance gain is due to Bayesian inference, which is able to account for different gene roles such as hubs. This suggests the possibility of replacing correlation based methods with their FPR estimation counterparts in future inference of genetic regulations.
- The new test P performed better than correlation test P_0 . This is the first comparative study to demonstrate the effect of genotype information in the inference of gene regulatory relations.
- The traditional causal inference test performed worse than random predictions. This confirms with real data that the indirect secondary test fails to identify true but weak regulations. The independence test had negligible effect as the sample size is small (not shown in Figure S5).
- Findr achieved higher AUROC and AUPR than all other methods attempted. It was also much faster than all other methods, especially CIT which also includes genotype data.
- Findr obtained a lower precision than lasso and elastic-net at small recalls. This might be explained by the fact that Lasso and elastic-net are multi-variate methods which incorporate all other gene expression levels besides pairwise information, and therefore exclude indirect regulators better.

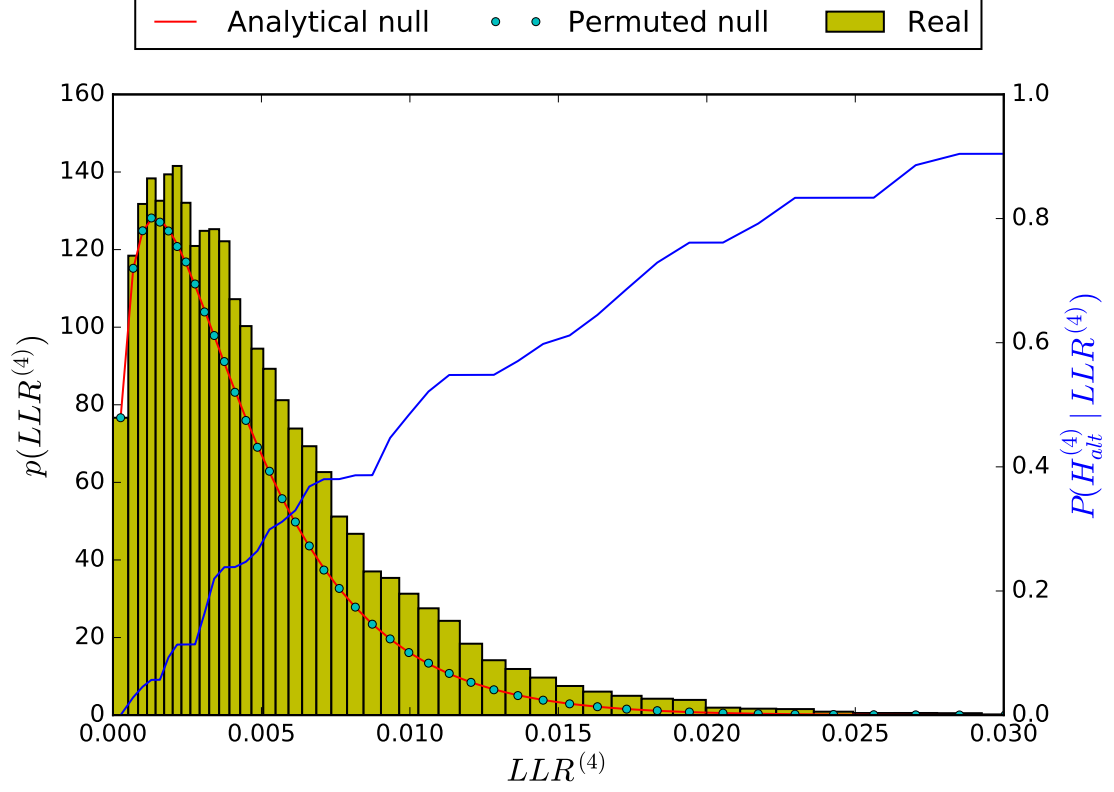


Figure S1: LLR distributions of the relevance test for hsa-miR-200b-3p on 23722 potential targets of Geuvadis dataset. Real, analytical null, and permuted null distributions are demonstrated in the figure, together with the curve of inferred posterior probability of alternative hypothesis. Permutations were randomly conducted on all potential target genes for 100 times. The alignment between analytical and permuted null distributions and the consistent incremental trend of posterior probability verify our method in deriving analytical null distributions.

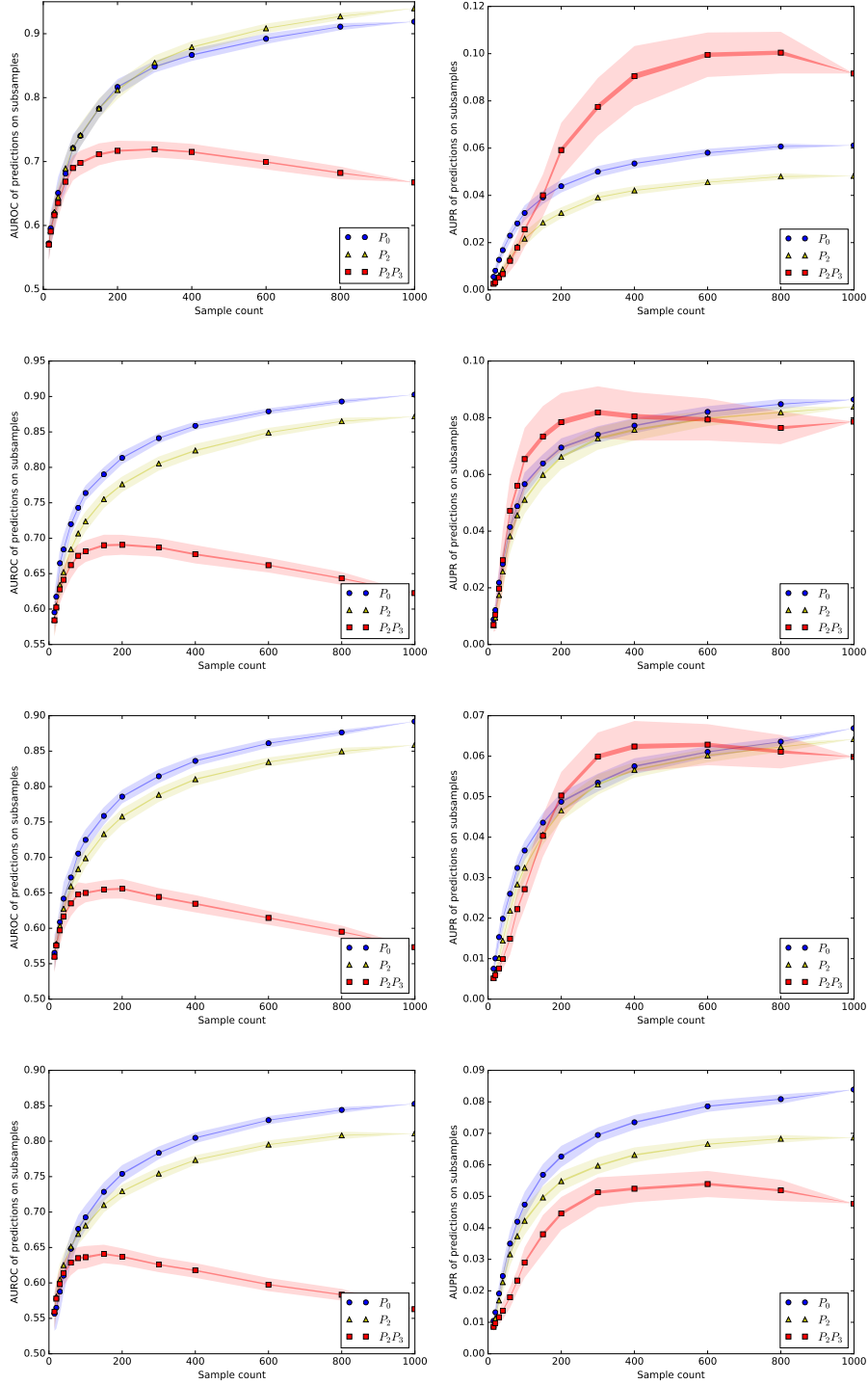


Figure S2: The mean AUROC and AUPR on subsampled data are shown for Trigger’s original causal inference together with the baseline correlation test. Every marker corresponds to the average AUROC or AUPR at specific sample sizes. Every sample size underwent 100 subsampling. Half widths of the lines and shades are the standard errors and standard deviations respectively, of AUROC or AUPR. Figures from top to bottom correspond to datasets 1, 2, 3, 5. For dataset 4, see Figure 1.

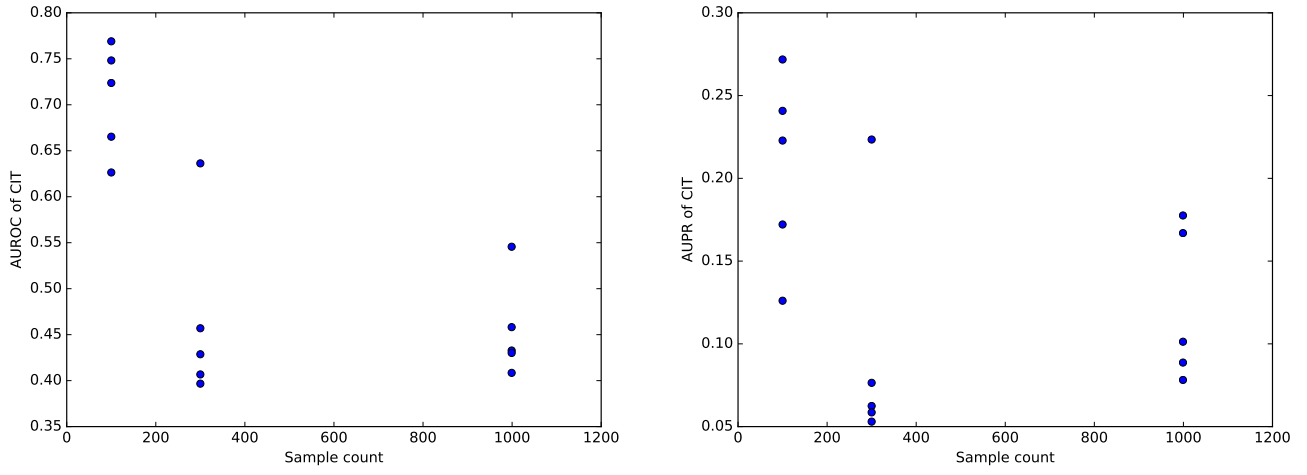


Figure S3: The AUROC and AUPR of CIT are shown for all 15 datasets of DREAM challenge. Every marker corresponds to the AUROC or AUPR of one dataset.

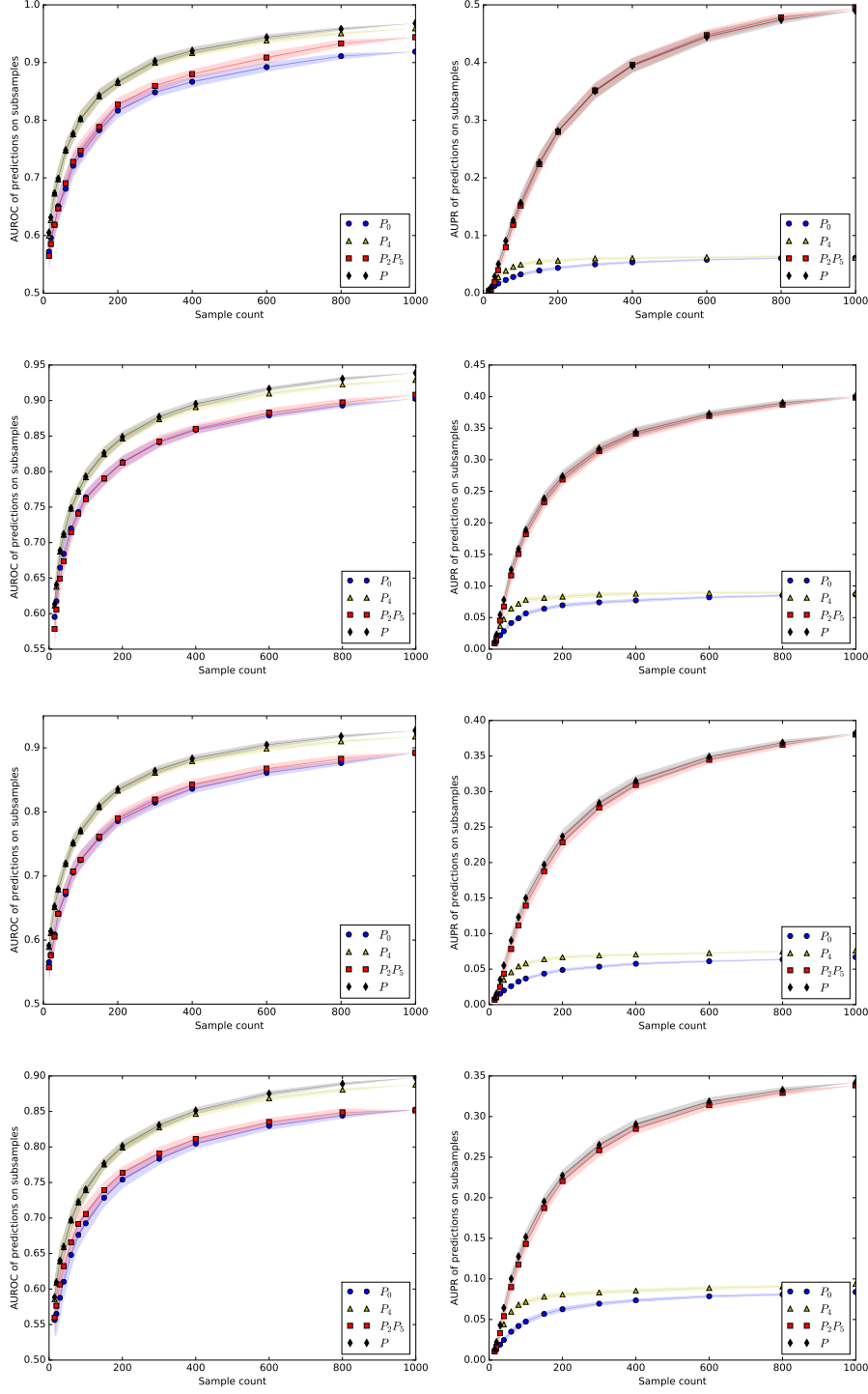


Figure S4: The mean AUROC and AUPR on subsampled data are plotted for causal inference with alternative tests, together with the baseline correlation test. Every marker corresponds to the average AUROC or AUPR at specific sample sizes. Every sample size underwent 100 subsampling. Half widths of the lines and shades are the standard errors and standard deviations respectively, of AUROC or AUPR. P is the recommended composite test defined in Eq 25, which achieves better performance than either individual test. Figures from top to bottom correspond to datasets 1, 2, 3, 5. For dataset 4, see Figure 3.

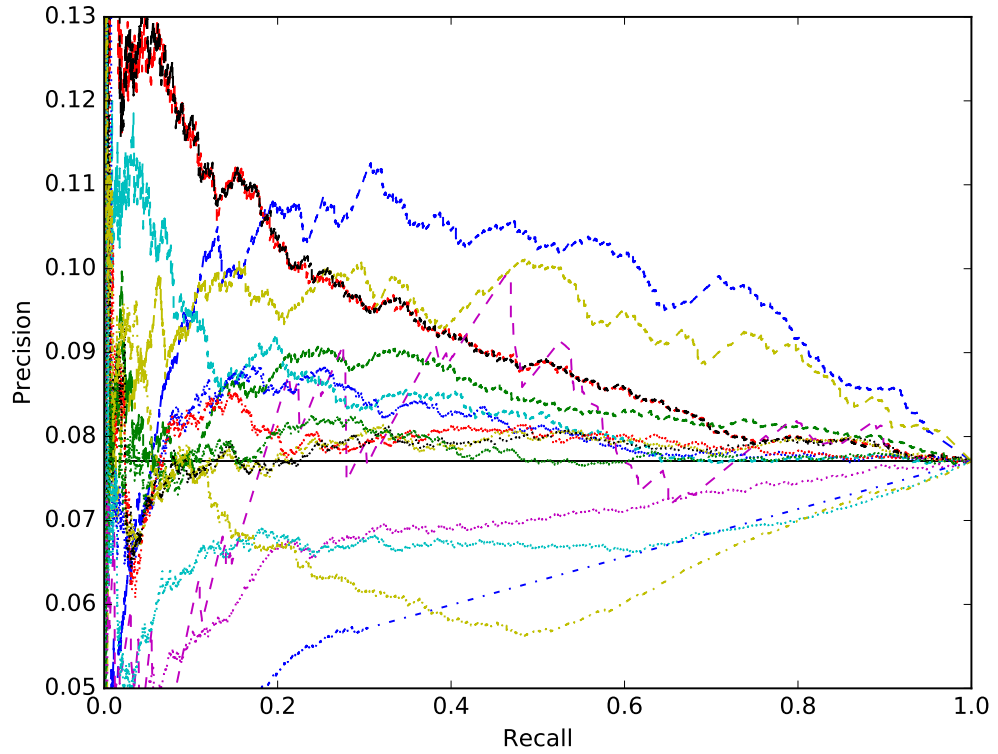
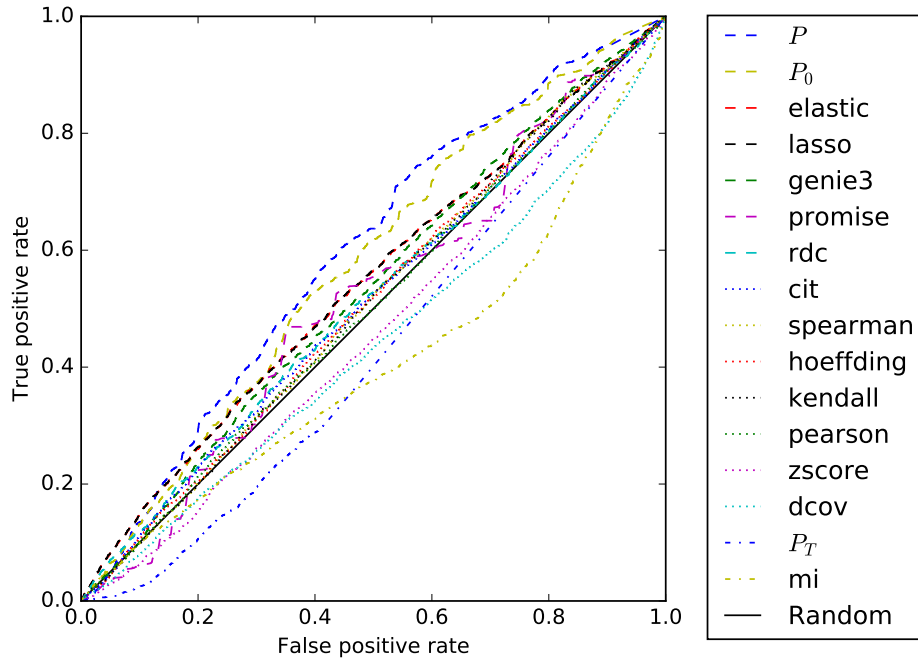


Figure S5: ROC and PR curves of miRNA target predictions are compared for Findr's traditional, new, and correlation tests, GENIE3, CIT, and 11 methods in miRLAB, based on Geuvadis data. The solid black lines correspond to performances from random predictions. A higher curve indicates better prediction performance.

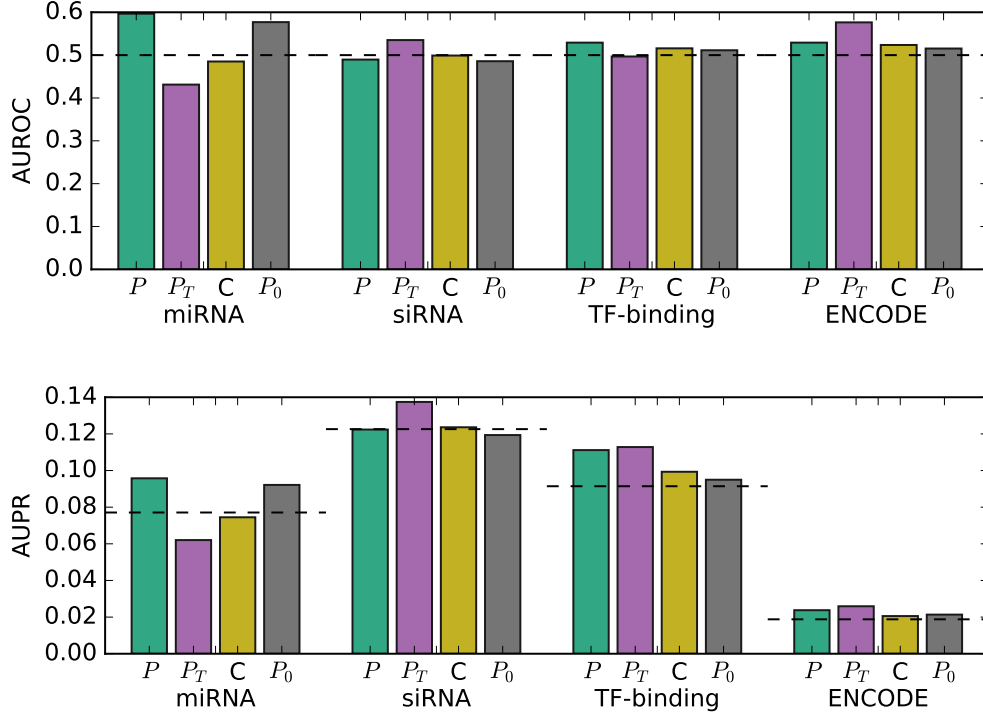


Figure S6: Three methods of causal inference are evaluated and compared against the baseline correlation test method (P_0): Findr's new test (P), traditional causal inference test (P_T), and CIT (C). AUROC and AUPR metrics are measured for three inference tasks. MiRNA compares miRNA target predictions based on Geuvadis miRNA and mRNA expression levels against groundtruths from miRLAB (Section 3.3). SiRNA and TF-binding compares gene-gene interaction predictions based on Geuvadis gene expression levels against groundtruths from siRNA silencing and TF-binding measurements in [21] respectively (Section 3.4). ENCODE compares the same gene-gene interaction predictions against TF-binding networks derived from ENCODE data [23]. Dashed lines indicate performances from random predictions.

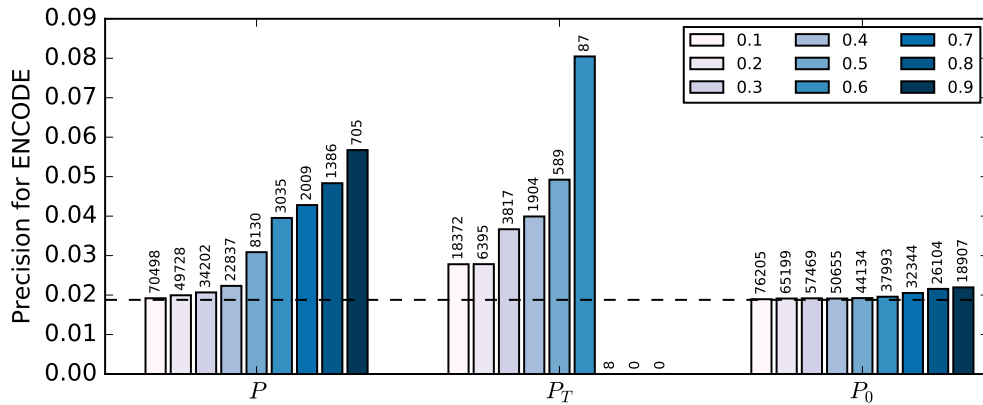


Figure S7: Inference precision at estimated TPR cutoffs 0.1 to 0.9 (light to dark) with respect to groundtruth network derived from TF binding of 14 TFs from ENCODE data [23]. The number above each bar indicates the number of positive predictions at the corresponding threshold. The dashed line is the precision from random predictions.

Table S1: Predictions of Findr’s traditional (P_T), new (P), and correlation (P_0) tests, and CIT are compared against DREAM challenge leaders on AUROC and AUPR for all 15 DREAM datasets. All cis- and trans-genes are included. DREAM challenge constrained the maximum number of submitted regulations by 100,000, which were also applied in our evaluation. Findr’s new test consistently obtained higher AUROC and AUPR than all other methods, including the leaders of DREAM challenge.

Sample count	100 samples					300 samples					999 samples				
Test id	1	2	3	4	5	1	2	3	4	5	1	2	3	4	5
P AUROC	0.772	0.750	0.737	0.736	0.719	0.882	0.842	0.839	0.825	0.797	0.941	0.899	0.882	0.867	0.848
P_0 AUROC	0.709	0.706	0.706	0.699	0.700	0.843	0.798	0.803	0.792	0.766	0.905	0.870	0.850	0.837	0.813
P_T AUROC	0.617	0.609	0.597	0.574	0.572	0.647	0.594	0.581	0.592	0.573	0.616	0.611	0.570	0.616	0.565
CIT AUROC	0.585	0.582	0.571	0.548	0.569	0.630	0.586	0.575	0.574	0.566	0.614	0.640	0.594	0.614	0.577
Leader AUROC	0.754	0.718	0.699	0.694	0.688	0.861	0.793	0.799	0.769	0.757	0.933	0.885	0.845	0.828	0.813
P AUPR	0.222	0.183	0.172	0.161	0.155	0.421	0.326	0.279	0.264	0.258	0.547	0.368	0.366	0.342	0.333
P_0 AUPR	0.051	0.049	0.040	0.051	0.055	0.084	0.053	0.063	0.078	0.057	0.093	0.072	0.070	0.076	0.077
P_T AUPR	0.044	0.048	0.042	0.023	0.041	0.109	0.054	0.051	0.054	0.047	0.070	0.068	0.042	0.070	0.049
CIT AUPR	0.075	0.066	0.060	0.031	0.050	0.162	0.075	0.074	0.080	0.067	0.168	0.149	0.098	0.168	0.096
Leader AUPR	0.103	0.072	0.067	0.068	0.067	0.309	0.243	0.191	0.182	0.191	0.358	0.258	0.195	0.183	0.178

Table S2: AUROCs and AUPRs of miRNA target predictions are compared for Findr’s traditional, new, and correlation tests, GENIE3, CIT, and 11 methods in miRLAB, based on Geuvadis data. Higher AUROC and AUPR values signify stronger predictive power. Program running times have units in seconds (s), minutes (m), hours (h), or days (d). Findr outperformed other methods in statistical power and speed, with or without genotype information.

	P	P_0	elastic	lasso	genie3	promise	rdc	cit	spearman
AUROC	0.60	0.58	0.55	0.54	0.53	0.52	0.52	0.51	0.51
AUPR	0.096	0.092	0.092	0.092	0.083	0.078	0.083	0.080	0.078
Time	0.88s	0.30s	4.53m	4.47m	12.1h	2.37m	50.3m	7.5d	2.37m
	hoeffding	kendall	pearson	random	zscore	dcov	P_T	mi	
AUROC	0.51	0.51	0.50	0.50	0.46	0.44	0.43	0.41	
AUPR	0.079	0.078	0.078	0.077	0.068	0.068	0.062	0.068	
Time	16.3m	41.9m	2.27m	-	2.90m	4.42h	0.84s	23.1m	